Optimal CO_2-based syngas supply chain configurations in Europe
Insights into location and scaling

Wiltink, Thijmen; Ramírez, Andrea; Pérez-Fortes, Mar

DOI
10.1016/j.compchemeng.2025.109187

Publication date
2025

Document Version
Final published version

Published in
Computers and Chemical Engineering

Computers and Chemical Engineering 201 (2025) 109187

Contents lists available at ScienceDirect

Computers and Chemical Engineering

journal homepage: www.elsevier.com/locate/compchemeng

Optimal CO_2-based syngas supply chain configurations in Europe: Insights into location and scaling

Thijmen Wiltink [a,*], Andrea Ramírez [b], Mar Pérez-Fortes [a]

[a] Department of Engineering, Systems, and Services, Faculty of Technology, Policy, and Management, Delft University of Technology, Jaffalaan 5, 2628 BX Delft, the Netherlands
[b] Department of Chemical Engineering, Faculty of Applied Sciences, Delft University of Technology, Van der Maasweg 9, 2629 HZ Delft, the Netherlands

ARTICLE INFO

Keywords:
CO_2 electrolysis
Supply chain modelling
Optimization
Supply chain configurations
Location
Scaling

ABSTRACT

Syngas production via high-temperature co-electrolysis of CO_2 (CO_2E) shows great potential to reduce the reliance on fossil fuels within the chemical industry. This paper presents an optimization model (MILP) to investigate syngas production from CO_2 in the European chemical sector. The model assesses the economic performance of CO_2E in prospective supply chains and explores alternative supply chain configurations under different syngas market sizes. The results reveal that the optimal placement of the CO_2 electrolysis plant in the supply chain is co-located or decentralized at the product location. This configuration reduces the need for syngas transportation by delivering CO_2 to the demand site, which is typically more cost-effective. At a syngas market fulfillment of 2 %, the lowest levelized cost of syngas is achieved at 673 EUR_{2018}/tonne, with electrolysis plants averaging a production capacity of 100 ktonne syngas/year. This levelized cost is between 1.5 and 4 times higher than the fossil-based reference.

1. Introduction

The chemical industry is highly energy-intensive and primarily dependent on fossil fuels as feedstock and energy source. It accounts for circa 5 % of the total European CO_2 emissions (European Environment Agency, 2024). As a significant emitter, the chemical industry must devote itself to the collective goal of achieving net-zero emissions by 2050 (European Commission, 2019).

Carbon capture and utilization (CCU) technologies, like the electrochemical conversion of CO_2, can be part of the portfolio for a net-zero chemical industry (2024/62/COM (2024)). Via this route CO_2, water, and electricity can be converted into relevant value-added products such as synthesis gas or syngas (Bushuyev et al., 2018; Smith et al., 2019). It serves as a versatile platform for producing various chemical end-products and transportation fuels (Choe et al., 2022). Syngas can be used in a Fischer-Tropsch process, an essential route for defossilizing the chemical industry by utilizing non-fossil-based CO_2 (Jarvis and Samsatli, 2018; Rodin et al., 2020) and renewable electricity (Schiffer and Manthiram, 2017). These two elements form the backbone of a supply chain (SC) designed to produce products with a reduced CO_2 footprint, outperforming existing benchmark processes (Sorknæs et al., 2022). This highlights that, in addition to technology development, integrating CO_2 electrolysis into the SC is essential for reducing the environmental impact while remaining cost-competitive.

Carbon dioxide electrochemical conversion into syngas can be executed at near ambient temperatures (low-temperature electrochemical CO_2 reduction or electrolysis, LT CO_2E) (Raya-Imbernón et al., 2024) or at high temperatures (high-temperature CO_2 electrolysis or HT CO_2E), above 700 °C (Deka et al., 2020). This work focuses on syngas production via HT co-electrolysis, which is currently in the demonstration and scale-up phase (technology readiness level (TRL) 5-6) (Detz et al., 2023). In HT co-electrolysis, both steam and CO_2 are converted into syngas.

Syngas is currently used as a short-lived intermediate, produced on-site using natural gas or coal. As an intermediate, syngas plays a crucial role in a broader SC, which typically consists of five stages: (i) feedstock sourcing, (ii) feedstock logistics, (iii) conversion, (iv) product logistics, and (v) end-use (Chandra and Grabis, 2016). In Europe, the main end-use of syngas is currently methanol production, with capacities ranging from 0.2 to 1.2 Mtonne methanol/year (ICIS, 2023a). Large-scale syngas supply chains are non-existent, and syngas is not directly sold as a traded commodity chemical (Schreiber et al., 2020). There are several reasons why syngas is not traded as a commodity. Hydrogen and carbon monoxide are highly flammable; hydrogen is prone to leak, and carbon monoxide is toxic (Al Ghafri et al., 2022;

* Corresponding author.
E-mail addresses: T.J.Wiltink@TUDelft.nl (T. Wiltink), M.D.M.Perez-Fortes@TUDelft.nl (M. Pérez-Fortes).

https://doi.org/10.1016/j.compchemeng.2025.109187
Received 21 November 2024; Received in revised form 8 April 2025; Accepted 11 May 2025
Available online 18 May 2025

Nomenclature

Indices

(c^*, c^*) Placeholders for CO_2 capture and transport-related sets: when these indices are encountered, the formulation applies to the listed set combinations. $\mathscr{C}^{Ci}$, $\mathscr{C}_i \vee \mathscr{C}^{Eh}$, $\mathscr{E}_h \vee \mathscr{C}_i$, $\mathscr{E} \vee \mathscr{E}_h$, $\mathscr{E}$

($CO2^*$, $CO2^*$) Placeholders for CO_2 transport-related sets: when these indices are encountered, the formulation applies to the listed set combinations. $\mathscr{C}^{Eh}$, $\mathscr{E}_h \vee \mathscr{C}_i$, $\mathscr{E} \vee \mathscr{E}_h$, $\mathscr{E}$

(t^*, t^*) Placeholders for all gas transport-related sets: when these indices are encountered, the formulation applies to the listed set combinations. $\mathscr{C}^{Eh}$, $\mathscr{E}_h \vee \mathscr{C}_i$, $\mathscr{E} \vee \mathscr{E}_h$, $\mathscr{E} \vee \mathscr{E}$, $\mathscr{S}$

Sets

Point sets

$\mathscr{C}$ Supply set – all the CO_2 sources in the model; indexed by *c – 1 .. 1573*

$\mathscr{C}_i$ All the individual CO_2 sources which are not part of a 25-km cluster; indexed by *ci – 1, .., 256*

$\mathscr{C}^{Ci}$ Subset – All the individual CO_2 sources (*cci*) in the model that are not part of a 25-km cluster; indexed by *c*

$\mathscr{C}^{Eh}$ Subset – All the exclusive hub CO_2 sources (*ceh*) which are part of a 25-km cluster; indexed by *c*

$\mathscr{E}_h$ All the exclusive hub CO_2 sources which are part of a 25-km cluster; indexed by *eh – 1, .., 481*

$\mathscr{E}$ All the possible electrolysis plant locations, consisting of CO_2 source locations, syngas demand points, and intermediate hub locations; indexed by *e – 1, .., 1071*

$\mathscr{S}$ All the direct and indirect syngas demand locations in the system; indexed by *s – 1, .., 54*

$\mathscr{P}^{Ci}$ Cartesian product – Links the CO_2 sources $\mathscr{C}^{Ci}$ to $\mathscr{C}_i$; indexed by *cci, ci*

$\mathscr{P}^{Eh}$ Cartesian product – Links the CO_2 sources $\mathscr{C}^{Eh}$ to exclusive hub $\mathscr{E}_h$; indexed by *ceh, eh*

Financial set

$\mathscr{X}$ Different expenditures of gas transport (CO_2 and syngas), CO_2 compression and CO_2 conversion; indexed by *pex – "total", "opex", "capex"*

Piecewise linearization sets

$\mathscr{B}$ The number of binary variables for mapping breakpoints (q) to segments (k); indexed by *b – 1 .. 3* – $(1, .., log_2(\mathscr{Q} - 1)\rceil)$

$\mathscr{B}01$ The number with the binary variables; indexed by *b01 – 0, 1*

$\mathscr{M}$ Type of piecewise linear data stored about the electrolysis plant; indexed by *m – "module", "cost"*

$\mathscr{T}$ Type of piecewise linear data stored about transport and capture; indexed by *f – "flow", "cost"*

$\mathscr{K}$ Segments of the piecewise linear cost function – Transport, capture, and compression; indexed by *k – 1, .., 8* – $(1, .., (\mathscr{Q} - 1))$

$\mathscr{K}_q$ Cartesian product – Contains the breakpoint and segment mapping, which is True for the two breakpoints (q) belonging to segment (k); indexed by *k, q*

$\mathscr{Q}$ Breakpoints of the piecewise linear cost function – for transport, capture, and compression; indexed by *q – 1, .., 9* – $(1, .., \mathscr{Q})$

Capture and compression sets

$\mathscr{I}^{Cc}$ Gray encoded Boolean incidence matrix that indicates if breakpoint (q) is part of segment (k) that has binary digit (b) equal to value (*b01*) – Specific for capture; indexed by *c, b, b01, q*

$not\mathscr{I}^{Cc}$ Opposite of the Boolean incidence matrix $\mathscr{I}^{Cc}$; indexed by *c, b, b01, q*

$\mathscr{L}^{Cc}$ Responsible for tracking the number of pieces of a capture and compression cost function; indexed by *tc, q*

$\mathscr{T}_c$ All the capture and compression technologies in the model-specific for each CO_2 source; indexed by *tc – "Compression", "Waste", "PP"*

$\mathscr{P}^{Cc}$ Cartesian product – All the CO_2 sources with their respective capture technology; indexed by *c, tc*

$\mathscr{C}^{Cap}$ Subset – Indicates whether a CO_2 source requires capture and compression from waste or pulp and paper; indexed by *c*

Transport sets

$\mathscr{I}^{T}$ Gray encoded Boolean incidence matrix that indicates if breakpoint (q) is part of segment (k) that has binary digit (b) equal to value (*b01*) – Specific for transport; indexed by t^*, t^*, *b, b01, q*

$not\mathscr{I}^{T}$ Opposite of the Boolean incidence matrix $\mathscr{I}^{T}$; indexed by t^*, t^*, *b, b01, q*

$\mathscr{L}^{BP}$ Tracking the number of pieces of a piecewise linear transport cost function; indexed by t^*, t^*, *q*

$\mathscr{L}^{Flow}$ Tracking whether a $\mathscr{L}^{Bp}$ cost function exists; indexed by t^*, t^*

Electrolysis sets

$\mathscr{L}^{Ele}$ Gray encoded Boolean incidence matrix that indicates if breakpoint (q) is part of segment (k) that has binary digit (b) equal to the value (*b01*) – Specific for the electrolysis plant; indexed by *e, b, b01, q*

$not\mathscr{I}^{Ele}$ Opposite of the Boolean incidence matrix $not\mathscr{I}^{Ele}$; indexed by *e, b, b01, q*

Parameters

Scalars - Fixed

BM^{Cost} 10.9 - The base module cost, cost of the standard module, [$MEUR_{2018}$/module]

FS 0.20 - Fraction of the CAPEX, which is attributed to the stack, [-]

CRF^{Plant} 0.10 - Capital recovery factor based on 20-year lifetime and 8 % interest, [-]

CO_2^{Conv} 0.73 - Conversion factor to transform CO_2 flow into syngas flow, [(Mtonne Syngas/year)/(Mtonne CO_2/year)] or [-]

E^{Conv} 7.1 - Electricity consumption of the electrolyzer due to the conversion, [MWh/tonne syngas]

E^{Bop} 2.1 - Electricity consumption of the electrolysis plant due to the balance of plant, [MWh/tonne syngas]

LT^{Stack} 5 - Lifetime of the electrolyzer stack, [year]

$MRK^{Fulfill}$ 13.9 - Flow of syngas produced yearly in the total supply chain, [Mtonne syngas/year]

MOD^{Flow} 0.0078 - Syngas flow produced per module per year, [Mtonne syngas/module/year]

OM^{Use} 0.04 - Fraction operations and maintenance as a function of the CAPEX, [-]

W^{Conv} 0.86 - Conversion factor to transform CO_2 flow into water flow, [(Mtonne water/year)/(Mtonne CO_2/year)] or [-]

Scalars – changed with different scenarios

CO_2^{y} Material yield factor to deal with CO_2 losses in the CO_2 conversion to syngas [-]

EC^{Cost} Electricity cost, [EUR_{2018}/MWh]

$CONV^{Elyzr}$ Electrolysis plant electricity consumption for the

conversion of CO_2 into syngas, [EUR_{2018}/Mtonne syngas]

BOP^{Elyzr} Electrolysis plant electricity consumption for the balance of plant, [EUR_{2018}/Mtonne syngas]

FR^{All} Upper fraction of CO_2 captured at the source applicable to all sources, [-]

FR_{tc}^{Bio} Fraction of CO_2 from each capture technology *tc* that is considered biogenic, [-]

FR^{Low} Lower fraction of CO_2 captured at the source, [-]

FR^{Up} Upper fraction of CO_2 captured at the source, [-]

LR The cost improvements due to learning in a 2040 scenario, [-]

MRK^{Fr} Varied Fraction of the total syngas demand that needs to be fulfilled, [-]

Tables

$CC_{tc,fc,q}^{Pwl}$ Piecewise linearization using breakpoints (*q*) of capture and compression (*tc*) for cost and flows (*fc*), three-dimensional

$CO2_{c,tc}^{In}$ Available CO_2 at the point sources in set (c), that is captured with capture and compression technology (*tc*), two-dimensional

$EPC_{m,q}^{Pwl}$ Piecewise linear data using breakpoints (*q*) about the investment cost of the electrolysis plant (*m*), two-dimensional

$GRAY_{k,\ b}$ Gray encoding to link segments (*k*) to binary variables (*b*)

SG_s^{Demand} Syngas demand at given locations in [Mtonne/year] at syngas demand location (s), one-dimensional

$T_{f,t^*,t^*,q}^{Pwl}$ Piecewise linearization using breakpoints (q) of all the transport segments ($_{t^*,\ t^*}$) for cost and flows (f), four-dimensional

Variables

Binary variables

$\delta_{e,b}^{Elyzr}$ Segment encoding using set (*b*) for the piecewise linearization of the electrolysis plant (*e*), [-]

$\delta_{tc,c,b}^{CC}$ Segment encoding using set (*b*) for the piecewise linearization of capture (*tc*) at source (*c*), [-]

$\delta_{t^*,t^*,b}^{T}$ Segment encoding using set (*b*) for the piecewise linearization of transport between transport links, [-]

cap_c^{Bound} Defined to create a semi-continuous variable for the minimum capture fraction of CO_2 at waste and pulp and paper sources (*c*), [-]

Integer variables

mod_e^{Nr} Number of modules installed per electrolysis plant (*e*), [# of modules]

Positive continuous variables

$\lambda_{tc,c,q}^{Cc}$ Interpolation using breakpoints (*q*) for the piecewise linearization of capture and compression at source EUR for the different capture technologies (*tc*), [-]

$\lambda_{e,q}^{Elyzr}$ Interpolation using breakpoints (*q*) for the piecewise linearization of the electrolysis plant EUR, [-]

$\lambda_{t^*,t^*,q}^{T}$ Interpolation using breakpoints (*q*) for the piecewise linearization of transport between transport segments ($_{t^*,\ t^*}$), [-]

cap_c^{Fr} The fraction of CO_2 that is captured from waste and pulp and paper CO_2 EUR, [-]

$cap_{c,x}^{Cost}$ CO_2 capture and compression cost (*x*) at source, [EUR_{2018}/year]

cap^{Tot} Total cost of CO_2 capture in the designed supply chain, [EUR_{2018}/year]

$ceheh^{Tot}$ Total transport cost of transporting CO_2 from the source (*ceh*) to the exclusive hub (*eh*), [EUR_{2018}/year]

cie^{Tot} Total transport cost of transporting CO_2 from the individual CO_2 source (*ci*) to electrolysis plant location, [EUR_{2018}/year]

$co_2flow_{c^*,c^*}$ Amount of CO_2 flow transported from source to destination, [Mtonne CO_2/year]

$co_2flow_c^{Cap}$ Amount of CO_2 captured from each CO_2 source (*c – cci, ceh*), [Mtonne/year]

ehe^{Tot} Total transport cost of transporting CO_2 from the exclusive hub (*eh*) to electrolysis plant location, [EUR_{2018}/year]

$elyzr_{e,x}^{Cost}$ Electrolysis plant cost (*pex*) at the electrolysis plant EUR, [EUR_{2018}/year]

$elyzr_e^{Elect}$ Electrolysis plant electricity cost at the electrolysis plant EUR, [EUR_{2018}/year]

$elyzr_e^{OM}$ Electrolysis plant operations and maintenance cost at the electrolysis plant EUR, [EUR_{2018}/year]

$elyzr_e^{Stack}$ Electrolyzer stack replacement cost at the electrolysis plant EUR, [EUR_{2018}/year]

$elyzr^{Tot}$ Total electrolysis plant cost, [EUR_{2018}/year]

es^{Tot} Total transport cost of transporting syngas from the electrolysis plant location EUR to the syngas demand location (*s*), [EUR_{2018}/year]

mod_e^{Cost} Total cost of the number of modules installed at the electrolysis plant (*e*) EUR, [EUR_{2018}/year]

$sgflow_{e,s}$ Amount of syngas flow transported from electrolysis plant (*e*) EUR to syngas demand location (*s*), [Mtonne syngas/year]

$t_{t^*,t^*,pex}^{Cost}$ Gas transport cost from source to destination, [EUR_{2018}/year]

$totsc^{Cost}$ The total cost of the supply chain elements capture, CO_2 transport, CO_2 conversion, and syngas transport, [EUR_{2018}/year]

Free continuous variables

$lcosg$ Objective variable – levelized cost of syngas production, [EUR_{2018}/tonne]

Abbreviations

BDO	Butanediol
BECCS	Bioenergy carbon capture and storage
CAPEX	Capital expenditures
CCS	Carbon capture and storage
CCU	Carbon capture and utilization
CEPCI	Chemical Engineering Plant Cost Indices
CO_2E	Co-electrolysis of CO_2
CRF	Capital recovery factor
DBSCAN	Density-based spatial clustering of applications with noise
EBA	European Biogas Association
EEA	European Economic Area
E-PRTR	European Pollutant Release and Transfer Register
FLP	Facility location problem
GAMS	General Algebraic Modeling System
HT	High-temperature
IEA	International Energy Agency
LCSOG	Levelized cost of syngas
LR	Learning rate
LT	Low-temperature

MDI	Methyleendifenyldi-isocyanaat	PP	Pulp and paper
MILP	Mixed integer linear programming	SC	Supply chain
MTBE	Methyl-tert-butylether	SOEC	Solid oxide electrolysis cells
NETL	National Energy Technology Laboratory	TIC	Total Investment Costs
O&M	Operation and maintenance	TRL	Technology readiness level
OPEX	Operational expenditures		

Stolecka and Rusin, 2020). For short distances, syngas is transported in the gas phase, and the most restrictive safety practices for H_2 and CO must be combined (European Industrial Gases Association AISBL, 2014). Hence, the effect of the transportation of syngas on supply chain configurations has not been explored (Ridjan, 2015). Due to the technical challenges and economic factors, plants in the syngas SC are typically co-located with their demand and depend on imported natural gas (or coal).

Carbon dioxide used for syngas production can be sourced from fossil fuels, biomass (Bui et al., 2021), waste conversion processes (Bisinella et al., 2021), or the atmosphere (Ostovari et al., 2023). Only the non-fossil-based sources are considered renewable by current regulations (2023/1184/EC and 2023/1185/EC (2023)). Under the right conditions, these CO_2 types can result in CO_2-neutral products (de Kleijne et al., 2022). Biogenic CO_2 could originate from biomass combustion, biomass digestion, biogas upgrading, industrial fermentation, and the production of pulp and paper (PP) (Onarheim et al., 2016; Rodin et al., 2020). Biogas upgrading and industrial fermentation result in highly CO_2-concentrated streams. These sources typically do not require costly carbon capture installations but do require compression before being transported (Bello et al., 2020). In Europe, there are over 1000 distributed biogas upgrading plants (European Biogas Association, 2023) that produce approximately 3.4 Mtonne CO_2/year (average size: 3 ktonne CO_2/plant per year) (Vieira, 2018). Bioethanol fermentation generates around 5 Mtonne CO_2/year; there are only 58 bioethanol fermentation plants in Europe, with an average size of 86 ktonne CO_2/plant per year (Lorenzo and Díaz, 2022). Waste incineration and PP contain around 10 volume % of CO_2 (Kearns, 2019; Onarheim et al., 2017), requiring both capture and compression before transport. In the E-PRTR (European Pollutant Release and Transfer Register (European Environment Agency, 2023)), the potential CO_2 emitted in Europe by waste incineration is 72 Mtonne CO_2/year (from 178 plants, with an average size of 404 ktonne CO_2/plant per year) and from PP, 88 Mtonne CO_2/year (from 267 plants, with an average size of 330 ktonne CO_2/plant per year).

Various CO_2 sources differ in average size and location, requiring careful alignment with the capacities and placements of CO_2 electrochemical conversion plants (and, in general, of any CCU plant). However, it is unknown how the geographical aspects determine whether the matching between CO_2 supply and CO_2-based syngas demand is feasible. Geographical aspects could significantly impact the costs and layout of the SC (Abdelshafy and Walther, 2022). CO_2 is commonly transported via pipeline or ship, with the choice depending on volume and distance (Bjerketvedt et al., 2022; d'Amore et al., 2021). Pipelines are most efficient for large flows in the dense phase (8–17 MPa), while gas-phase transport (1.5–3 MPa) is more suitable for smaller volumes and shorter distances (Knoope et al., 2014a, 2014b). Shipping can become more cost-effective under the right circumstances and over 500 kilometers (Smith et al., 2021). For these transport options, the increase in annual flow reduces the unit transportation costs in the SC due to economies of scale (Bennæs et al., 2024).

Centralized SCs benefit from economies of scale and shared infrastructure but depend on the cheap transportation of feedstocks and products, which makes them independent of local resources (Almena et al., 2019; Knauff, 1973). Decentralized SCs may use local resources, reducing transport costs. Small-scale SC configurations could align with CO_2 electrolysis due to its high level of modularity (Noordende et al., 2023). However, these plants may lose economies of scale, requiring alternative strategies for developing economically feasible SCs. Instead of scaling up, costs can be reduced through economies of number (Prosser et al., 2024), learning by doing, and economies of scale in manufacturing (Detz et al., 2023). Given the trade-off between production scale, location, and transport costs, models are essential for optimizing CO_2E supply chains.

This work addresses three knowledge gaps to identify the most cost-effective configurations and sizes for electrolysis plants within a syngas SC:

(i) It is not yet fully understood at which scale CO_2-based syngas plants could be implemented to ensure a match between CO_2 supply and syngas demand.
(ii) It is unknown to what extent CO_2 electrolysis plants rely on the centralization and transportation of CO_2 and/or syngas.
(iii) There is a lack of understanding of the supply chain configuration schemes suitable for CO_2 electrolysis.

The following sections present the case study, provide an overview of the model's underlying data, and the methods used in Sections 2 through 4, respectively. Section 5 covers the mathematical formulation, with results and discussion in Section 6 and the conclusion in Section 7.

2. Case study description

A mixed integer linear (MILP) supply chain model was developed to explore a case study on syngas production from biogenic CO_2 for the European chemical industry across various scenarios. The European Economic Area (EEA), including Switzerland and the UK, was selected as the geographical scope. The choice of this geographic area avoids potential edge effects that could arise from excluding key CO_2 sources, syngas demand locations and connections; in other words, by considering the full European landscape, the model could identify the most promising regions for CO_2E.

The system was optimized from the perspective of a central planner who considers optimizing the whole supply chain, working as a unique decision-maker. This meant that the perspectives of individual stakeholders in the SC were not considered, and perfect collaboration between actors within a supporting context was assumed.

The focus was on biogenic sources of CO_2 since these sources will most likely remain applicable for CCU applications in the next 20 years. In contrast, fossil-based point sources are targeted to be phased out under current environmental policies (2023/1184/EC and 2023/1185/EC (2023)). Therefore, the current case study included CO_2 from biogas upgrading, bioethanol fermentation, PP, and non-hazardous waste incineration. This paper did not explicitly consider other inputs, like renewable electricity and water, which were assumed to be available at the locations in the required amounts.

The case study was based on data from 2018 to 2023 regarding prices, CO_2 availabilities, and syngas demands. The CO_2 supply and syngas demand were assumed to be constant throughout the year and across the years. All the investments were assumed to be made in 2020. The investment costs for the electrolyzer were projected for 2030, reflecting a TRL of 9 and matching the maturity level of the surrounding

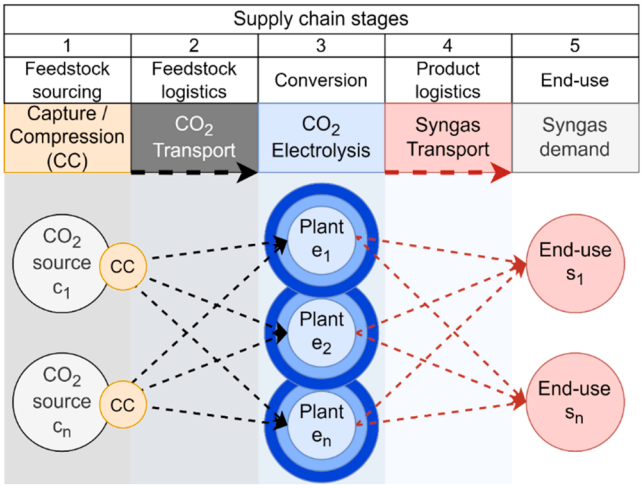

Fig. 1. Considered supply chain stages. The case study has pre-defined CO_2 sources and syngas consumers. End-use considers the current demand for syngas in the European chemical industry.

supply chain echelons. The resulting supply chain configurations were designed to minimize the levelized cost of syngas (LCOSG) production while meeting syngas market demand.

This case study examined all stages of a typical supply chain (see Fig. 1). The first stage involved feedstock sourcing, including CO_2 sources and their capture and compression. In the second stage, CO_2 was transported via pipeline to the conversion location. This was the only transport mode considered. The transportation distance and the CO_2 flow affected the transportation cost to the electrolysis plant. At the conversion stage, CO_2 was converted into syngas. The conversion cost depended on the flow of syngas produced. The electrolysis plant could be placed in one of three possible locations: (i) at the feedstock sourcing location, (ii) at a pre-defined location between the feedstock sourcing and the end-use, or (iii) at the end-use location. Finally, the syngas could be transported via pipeline to meet the demand at the end-use stage. The syngas flow quantity was bound by demand fulfillment requirements. Different percentages of the total market demand fulfillment were used as input to investigate the impact of varying market penetrations on the SC configuration. Achieving a larger syngas market is a gradual process; the lower market percentages illustrated the role of CO_2E as it transitions from a niche technology to one with industrial relevance through technology deployment and scaling.

Various supply chain configurations and electrolyzer sizes were explored, and the case study was evaluated under four scenarios categories: (i) changes in electricity prices, (ii) variation in fulfilling the syngas demand, (iii) reduction in investment costs, and (iv) changes in process efficiencies. The first two scenarios addressed changes in system input and output hypotheses. The latter two focused on potential enhancements, cost reductions, and modifications within the capture and conversion units.

3. Model data overview

3.1. Feedstock sources and product demand

3.1.1. CO_2 sources

Data regarding the specific location and amount of CO_2 emitted from waste incinerators and pulp and paper plants was retrieved from the European Pollutant Release and Transfer Register (E-PRTR). The threshold value to report CO_2 emissions is 0.1 Mtonne/year; therefore, given the size of these plants, they are well-represented in the database.

Different databases were needed to investigate the size of biogas and bioethanol plants, as they are usually smaller than the E-PRTR report limit. The European Biogas Association (EBA) states that more than 19,000 biogas plants are operational in Europe (European Biogas Association, 2023). A small fraction (around 5 %) of them upgrade biogas into biomethane, yielding highly concentrated CO_2 (Rodin et al., 2020). The biomethane plants data was retrieved from the International Energy Agency (IEA) Task 37 biomethane plant list of 2020 and the biomethane map of 2021 made by the EBA (European Biogas Association and Gas Infrastructure Europe, 2021; IEA Bioenergy Task 37, 2020). The data from these sources was merged and georeferenced. Overall, 1077 biomethane plants were identified. These biomethane plants collectively produce 4.7 Mtonne CO_2 per year, as summarized in Table 1. Seven bioethanol plants were found using the E-PRTR and the ICIS chemical profile of ethanol (ICIS, 2020). The IEA Bioenergy Task 39 (2023) lists bioethanol plants at varying TRL levels; only bioethanol plants with a TRL higher or equal to eight were retrieved from this database. The list was completed using the CO_2 source identification report of Lorenzo and Díaz (2022). Only the high-purity CO_2 stream from the fermentation was considered in the SC model. Therefore, it was assumed that in a bioethanol plant, only 43 % of the CO_2 originates from this section of the plant (Laude et al., 2011). Table 1 summarizes the size characteristics of the different CO_2 sources considered in the model. The CO_2 figures in Table 1 correspond to pure CO_2 flows.

Fig. 2 locates the individual CO_2 sources in the European territory and aggregates them per NUTS-2 region. In Scandinavian countries, particularly Sweden and Finland, large volumes of biogenic CO_2 (3-9 Mtonnes/year) are produced by PP plants. In Portugal's central region, a significant PP industry has a potential of 4.8 Mtonnes of CO_2 annually. In Western Europe, combinations of waste incinerators and PP plants provide a CO_2 potential of 0.5–1.5 Mtonnes/year per NUTS-2 region. Biomethane and bioethanol plants are widely distributed across the case area.

3.1.2. Syngas demand

Europe's current direct syngas demand is reported in Fig. 3 and originates from the synthesis of ethanol, oxo-alcohols, butanediol (BDO), and methanol (ICIS, 2023b, 2023a, 2022, 2017). The demand from methanol derivatives was also included, increasing the syngas demand within the case study. The products considered from this derived demand were MTBE (Methyl-tert-butylether), formaldehyde, acetic acid, and MDI (methyleendifenyldi-isocyanaat) (Andersen et al., 2014; ICIS, 2023c, 2023d, 2018). Energy applications and chemical products that utilize only the hydrogen or carbon monoxide fraction of

Table 1
Sizes of the selected CO_2 sources in the case area.

Industry	Total CO_2 availability	Avg. plant CO_2 size	Max plant CO_2 size	Nr. of plants	Sources
	[Mtonne/year]	[ktonne/year]	[Mtonne/year]	[#]	
Bioethanol	2.3	51.4	0.228	45	a
Biomethane	4.7	4.39	0.0782	1077	b
Pulp and paper	88.1	495	3.04	178	c
Waste incineration	72.7	266	1.73	273	c

[a] ICIS (2020), IEA Bioenergy Task 39 (2023), Lorenzo and Díaz (2022). [b] European Biogas Association and Gas Infrastructure Europe (2021), IEA Bioenergy Task 37 (2020). [c] European Environment Agency (2023).

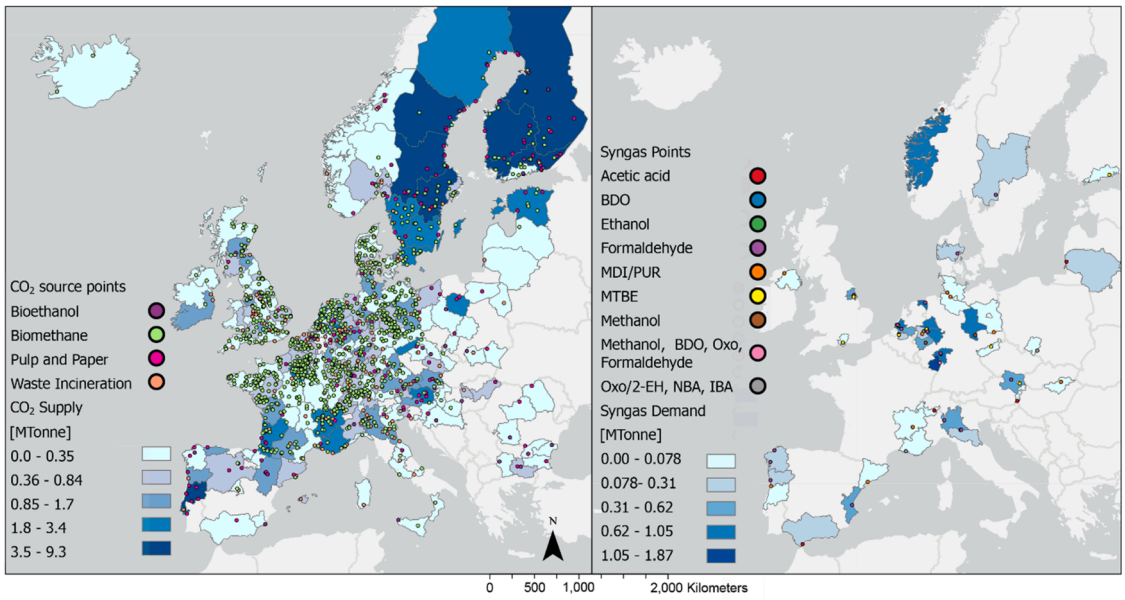

Fig. 2. Map of the biogenic CO_2 sources and yearly production – left. Map of the syngas users and yearly demand – right.

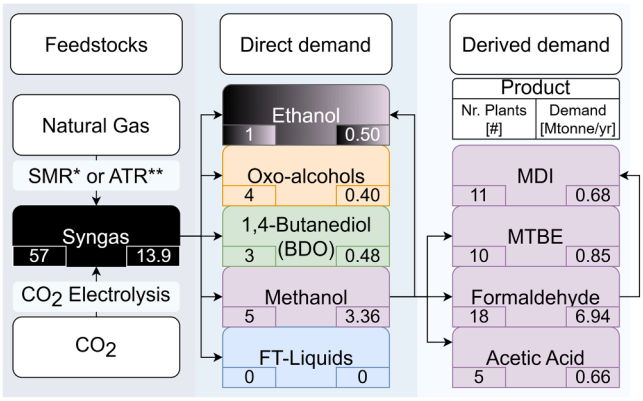

Fig. 3. Chemical end-products synthesized from syngas, both direct and derived demand. The left value represents the total number of plants in the case area, and the right value is the total syngas demand per year. *Steam Methane Reforming (SMR) **Autothermal reforming (ATR).

syngas were omitted in this analysis. The size of the syngas demand site was defined based on the plant capacity of the end-product. Based on these plant capacities, the amount of syngas consumed was calculated using stoichiometric reactions and reaction efficiencies, as further explained in SI 1. Each end-product requires a specific H_2/CO ratio in the syngas stream, which is between 1-2 for alcohol synthesis and around 2 for methanol (Cui et al., 2020). Methanol makes up the largest fraction of the syngas demand in the case area; therefore, as a simplification, an H_2/CO ratio of 2 was assumed for all end-products.

In total, 57 plants have a syngas demand of 13.9 Mtonne/year. The BASF site in Ludwigshafen and the Lyondell site in the Port of Rotterdam have multiple plants in the same location that utilize syngas for different products. Therefore, 53 unique syngas demand locations were considered.

Regarding the products' individual size, oxo-alcohols, and MDI typically have the smallest syngas demand per plant (in the 50–150 ktonne/year range). Methanol has the largest syngas demand, ranging from 300 to 1050 ktonne syngas annually. In Fig. 2, the different syngas demand locations are visualized and aggregated per NUTS-2 region. Germany has the highest syngas demand in Europe, with 5.8 Mtonnes per year, followed by the Netherlands with 2.3 Mtonnes per year. The syngas demand is mainly located around the Port of Rotterdam, the Ruhr

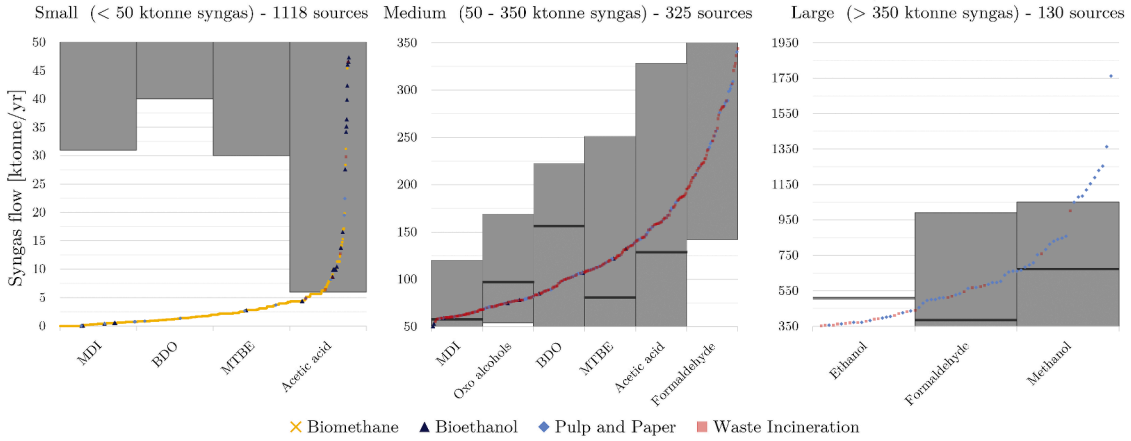

Fig. 4. The annual amount of syngas that could be produced from small, medium, and large-scale CO_2 sources compared to the syngas demand of various products.

area, and the BASF site in Ludwigshafen. The largest syngas demand point is identified in Norway, where methanol is produced with a syngas demand of 1.05 Mtonne syngas per year. Smaller syngas demand points are scattered around the UK, Central Europe, and the Iberian Peninsula.

3.1.3. Comparison between CO_2 sources and syngas demand scale

Fig. 4 compares the syngas production potential from CO_2 sources in Europe with the syngas demand for various products without considering the geographical aspect. Fig. 2 shows that locations with a large CO_2 availability (over 3 Mtonne/year) differ from locations with a large syngas demand (over 1 Mtonne/year). The grey area indicates the minimum and maximum size of the syngas-derived end-products, and the black bar indicates the average product size expressed as syngas demand. The points for the CO_2 sources in Fig. 4 are sorted based on the amount of syngas that could be produced with the emitted amount of CO_2. The small tier (< 50 ktonne syngas/year) was selected to include all biomethane CO_2 sources. In comparison, the largest tier (> 350 ktonne syngas/year) represented the end-products with the three highest average syngas demands. The syngas flow on the y-axis continues through the different tiers from left to right in Fig. 4.

The lowest syngas demand was identified from an acetic acid plant (6 ktonne syngas/year). Only 25 % of the biomethane sources could supply the required amount of CO_2 for this demand (one-to-one), indicating that 75 % of these sources were too small to meet the minimal syngas demand. These mini sources were insufficient to meet industrial syngas demand without clustering. Different bioethanol plants matched in scale with a range of different syngas-derived end-products. Only formaldehyde and methanol plants were generally too large to be matched with CO_2 from bioethanol plants. Waste incineration and PP plants varied widely in the amount of CO_2 emitted. Therefore, one-on-one matches with all the end-products were possible. These plants were large enough to supply the amount of CO_2 needed for syngas required by a methanol plant.

3.2. Capture and compression

The model included four types of CO_2 sources, each with their specific capture and compression needs. The modeling methodology of Hasan et al. (2014, 2012) was followed for the cost equations regarding the CO_2 capture of PP and waste incineration (the low-concentration CO_2 sources in the model). For the compression of CO_2 from bioethanol and biomethane plants (the high-concentration CO_2 sources), the CO_2 compression cost model by McCollum and Ogden (2006) was used. That cost model is applied for large-scale CO_2 compression (above 320 ktonne/year). Since small-scale sources like bioethanol and biomethane did not reach the minimum flow from this large-scale window, we verified the applicability of the cost function to smaller-scale operations.

- Bioethanol plants have a broad range of CO_2 flow sizes, ranging from 20 to 250 ktonne annually. The report from the National Energy Technology Laboratory (NETL) by Hughes et al. (2022) included a sensitivity analysis between the CO_2 emission size and the cost of compression for ethanol plants. Similar outcomes were generated with the methods used in both this work and theirs; see SI 2.
- Biomethane plants range between 0 and 75 ktonne CO_2/year. The cost of CO_2 compression for biomethane was verified using Wilkes et al. (2023) work, which modeled the CO_2 compression from an open-cycle gas turbine with a CO_2 flow of 11 ktonne/year. Also, comparable costs were found for this single capacity (no other literature source was found reporting CO_2 compression costs below 100 ktonne CO_2 per year).

3.3. Gas transport and terrain factors

The CO_2 and syngas transport costs were based on the CO_2 transport cost model of the National Energy Technology Laboratory (Morgan et al., 2023). In this model, data about several pipeline characteristics can be simulated regarding (i) the minimum inside pipe diameter, (ii) the number of pumps, (iii) the annual pump energy usage, (iv) the total operation and maintenance (O&M) costs, (v) the total capital costs, (vi) the annualized capital expenditures (CAPEX), (vii) the annualized operational expenditures (OPEX) and (viii) the total annualized cost. The minimum allowed pipeline diameter for CO_2 and syngas was 4 in. (0.10 m), the same diameter threshold as in McCoy and Rubin (2008). This CO_2 cost model was also used to calculate syngas transport costs since, to our knowledge, no open-source syngas transport model is publicly available. It was adapted to account for differences in gas characteristics. The model used the cost parameters of CO_2, and physical parameters of syngas (with an H_2/CO ratio of 2), such as molecular weight, density, compressibility, and viscosity.

The pipeline investment cost highly depends on the terrain that needs to be crossed (Serpa et al., 2011). Therefore, data regarding terrain elements, such as slope (European Environment Agency, 2012), land cover (European Environment Agency, 2019a), existing pipeline corridors (Diettrich et al., 2021), nature reserves (European Environment Agency, 2021a, 2019b), and nationally designated nature areas (European Environment Agency, 2021b) were collected. The terrain data was transformed into a cost surface raster to correct the cost of the pipeline crossing a particular terrain. The same factors as van den Broek et al. (2013) were used to convert these terrain elements into a cost surface raster, see Fig. 5. The lighter shades indicate a lower cost for crossing the terrain with a pipeline, while darker shades correspond to higher costs.

3.4. Electrolysis plant

The electrolysis plant cost was based on Noordende et al. (2023) and Detz et al. (2023) (as summarized in Table 2). The standard module was assumed to be 9 MW and included the electrolyzer and the balance of

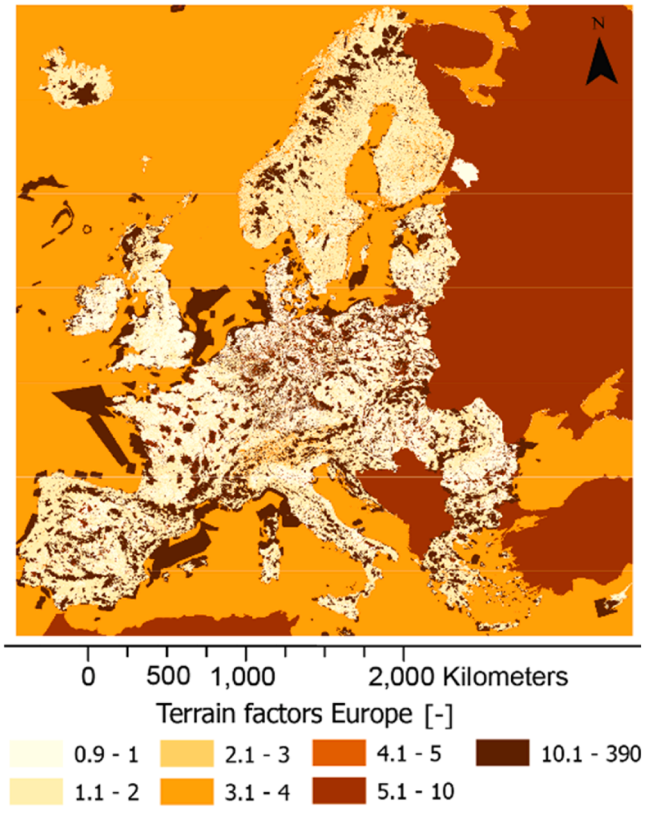

Fig. 5. Terrain cost surface raster used to determine transportation paths.

Table 2
Cost data, CO_2 input, syngas output, electricity consumption, operation and maintenance conversion factors in a 2030 scenario (Detz et al., 2023; Noordende et al., 2023).

	Value	Unit
Capital expenditures (CAPEX)	1214	EUR_{2018}/kW from 90 MW onwards
Total cost per module	10.9	$\cdot 10^6$ EUR_{2018} per module
Investment cost of stack	20	% of total CAPEX
Size of module	9	MW
Syngas production per module	7.82	ktonne syngas (H_2/CO ratio 2)/ module
CO_2 requirement per module	13.5	ktonne CO_2/module
Operation and maintenance	4	% of non-stack CAPEX
Electricity electrolyzer conversion	7.1	MWh/tonne syngas
Electricity balance of plant	2.1	MWh/tonne syngas
Total Electricity	9.2	MWh/tonne syngas

plant equipment (i.e., gas purification, electricity supply, and water treatment), as in Noordende et al. (2023).

To achieve plants larger than 90 MW, Noordende et al. (2023) proposed to repeat the same 10-module system. Based on this, we assumed that 90 MW is the threshold after which there are reduced benefits of economies of scale. We applied the 0.6-scaling rule to the initial ten modules, and beyond that, we assumed that the electrolysis plant scales linearly by number. For instance, we obtained that the first 9 MW module has a CAPEX of 4833 EUR_{2018}/kW. This value is within the upper and lower cost boundaries of 5338 - 2966 EUR_{2018}/kW, presented by Detz et al. (2023) using one ktonne syngas production/year as a reference scale. For more information about the cost function for the different numbers of modules used in this work, see Appendix I.

4. Methods

4.1. Pipeline distances, terrain factors, and clustered CO_2 sources

ArcGIS® Pro was used to compute the terrain-aware optimal paths for syngas or CO_2 pipelines between the different echelons. First, distance accumulation and back-direction rasters were generated from all starting points using the cost surface raster (Fig. 5). These rasters were then used to calculate the optimal paths between all points. Simultaneously, the distance of a pipeline path and the average terrain factor were calculated. Path generation was a highly automated process; therefore, some paths may have overlooked specific local conditions. Since distance accumulation raster calculations were highly computationally intensive given the European scope, the raster was resampled from 100 by 100 m to a resolution of 325 by 325 m.

To reduce the number of distance accumulation operations, clustering of CO_2 sources was applied. The point clustering geoprocessing tool in ArcGIS® Pro was used. Carbon dioxide sources were clustered using the DBSCAN method (Density-based spatial clustering of applications with noise (Ester et al., 1996)). If the points were within a defined radius of 25 km, a new starting point was placed in the middle of this cluster. When CO_2 sources were not part of a cluster, their original location was used as a starting point.

4.2. Piecewise linearization of non-linear input data

The investment in CO_2 compression, capture, transport, and the electrolyzer are described by non-linear cost functions. The cost functions were approximated using piecewise linearization to account for the non-linear economies of scale in a strictly linear model. The method proposed by Muggeo (2003) was used and implemented via the Python package by Pilgrim (2021). For CO_2 capture, compression, and transport, the non-linear cost functions were described using four pieces (five breakpoints). Eight pieces (nine breakpoints) were chosen for the conversion stage to balance model fit and performance for a cost function that combines both non-linear and linear parts. The first selected breakpoint was the cost function's origin, implying no costs without any flow.

Table 3
Overview of the seven scenarios (six variants and a base scenario) and parameter values.

Scenario name	Scenario category	Model param.	Base value	Scenario value	Unit
Elec20	1 - Changes in electricity prices	EC^{Cost}	45	20	[EUR_{2018}/MWh]
Elec70	1 - Changes in electricity prices	EC^{Cost}	45	70	[EUR_{2018}/MWh]
SGD1	2 - Variation in fulfilling syngas demand	SG_s^{Demand}	0.007–1.8	< 1	[Mtonne/year]
LR02	3 - Investment cost reduction	LR	0	0.8	[-]
CO_2Y1	4 – Changes in process efficiencies: CO_2 conversion	CO_2^Y	0.8	1	[-]
FrCap	4 – Changes in process efficiencies: CO_2 capture rates	FR^{All}	1	0.95	[-]
		FR^{Low}	0.75	0.65	[-]
		FR^{Up}	1	0.85	[-]

4.3. Scenarios

The case was evaluated under four different scenario categories, deriving into seven scenarios (including the base scenario; see Table 3). All these scenarios were evaluated under the same range of syngas demands that must be fulfilled. An overview of all the scenarios is presented in Table 3.

1 - Changes in electricity prices

In the base scenario, the electricity price was set at 45 EUR_{2018}/MWh, corresponding to the average non-household (IF band) EU electricity price in 2018 (Eurostat, 2024a). An optimistic and pessimistic scenario of 20 and 70 EUR_{2018}/MWh were evaluated to explore the effect of electricity pricing on the SC.

2 - Variation in fulfilling syngas demand

In the base scenario, the size of the syngas demand was derived from the demand for different end-products, as described in Section 3.1. The specific demand for each location ranges between 0.007 and 1.8 Mtonne/year. In this scenario, instead of capping the demand at the identified levels for each location, all syngas demand locations were allowed to produce up to 1 Mtonne syngas/year (which is approximately the highest syngas demand observed in Europe).

3 - Investment cost reduction

In Detz et al. (2023), investment costs decreased by 80 % in the 2040 scenario due to learning (LR). The same CAPEX reduction was assumed in this scenario, with the electrolysis plant CAPEX set at 20 % of the base scenario.

4 - Changes in process efficiencies: CO_2 conversion and CO_2 capture rates

Based on Noordende et al. (2023), an 80 % CO_2 conversion was assumed (CO_2^Y), meaning that 20 % of the CO_2 that is put into the electrolysis plant will not end up in the end product (assumption in our base scenario). However, Detz et al. (2023) used the theoretical maximum CO_2 conversion of 100 % (assumption in scenario CO_2Y1).

We assumed in the base scenario that all of the available CO_2 (FR^{All}) from a source could be captured/compressed. There was a minimum capture threshold of 75 % for waste and PP (FR^{Low}) to prevent the installation of undersized capture systems at large-scale point sources. There was no such lower capture threshold for the sources that only required compression. In the FrCap scenario, a capture range with a maximum of 85 % (FR^{Up}) and a minimum of 65 % (FR^{Low}) was set for PP and waste incineration sources (Haaf et al., 2020; Sagues et al., 2020). For the purer sources, an upper capture limit of 95 % (FR^{All}) was set (Cormos, 2014).

4.4. Supply chain configuration classification

For classification, we used three main configuration types: (i) co-location, (ii) decentralization, and (iii) centralization. This enabled us to compare different SC configurations and identify the preferred placement of the electrolysis plant. These types were further split into nine sub-types, as described in Fig. 6. A co-location boundary was introduced for the characterization of configurations. It is a pre-defined distance around the electrolysis plant (set at 10 km, which is large enough to contain large-scale chemical complexes such as the Botlek area in Rotterdam or the BASF site in Ludwigshafen). The position of the first and last SC echelons in relation to the electrolyzer and its co-location boundary ultimately determined the configuration type. Fig. 6 shows the specific requirements for each SC configuration. A SC configuration is co-located when both the feedstock supply and product demand fall within the co-location boundary. It is decentralized if the feedstock supply or product demand lies outside this boundary. Finally, centralized configurations have both the start and end of the supply chain outside the boundary.

To characterize the SC configurations, firstly, the SC configuration types of all the electrolysis plants in the system were categorized. Then, the percentage of each supply chain type was calculated.

Several software packages were necessary for processing and simulating input data, solving the mathematical model, and post-processing the optimization results, as shown in SI 7.

5. Model formulation

The SC model was defined as a fixed-charge facility location problem (FLP) (Laporte and Nickel, 2015), meaning there is a finite set of suppliers, plant locations, and demand points, see Fig. 1. All the possible connections between the suppliers, plant locations, and demand points were pre-defined. Using this approach, all configuration types defined in Section 4.4 were among the model options. The model was defined as a capacitated multiple allocation FLP. The capacitated aspect came from a constraint affecting the maximum size of the electrolysis plant. The echelons could connect to multiple other SC echelons through transport links. The model made four key decisions by minimizing the levelized

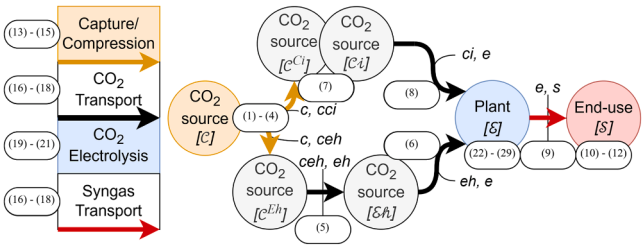

Fig. 7. Predefined order of the supply chain elements; the numbers in round brackets refer to the corresponding equations. Set names are in square brackets, and italicized text connect to the arrows indicates transport connections between sets.

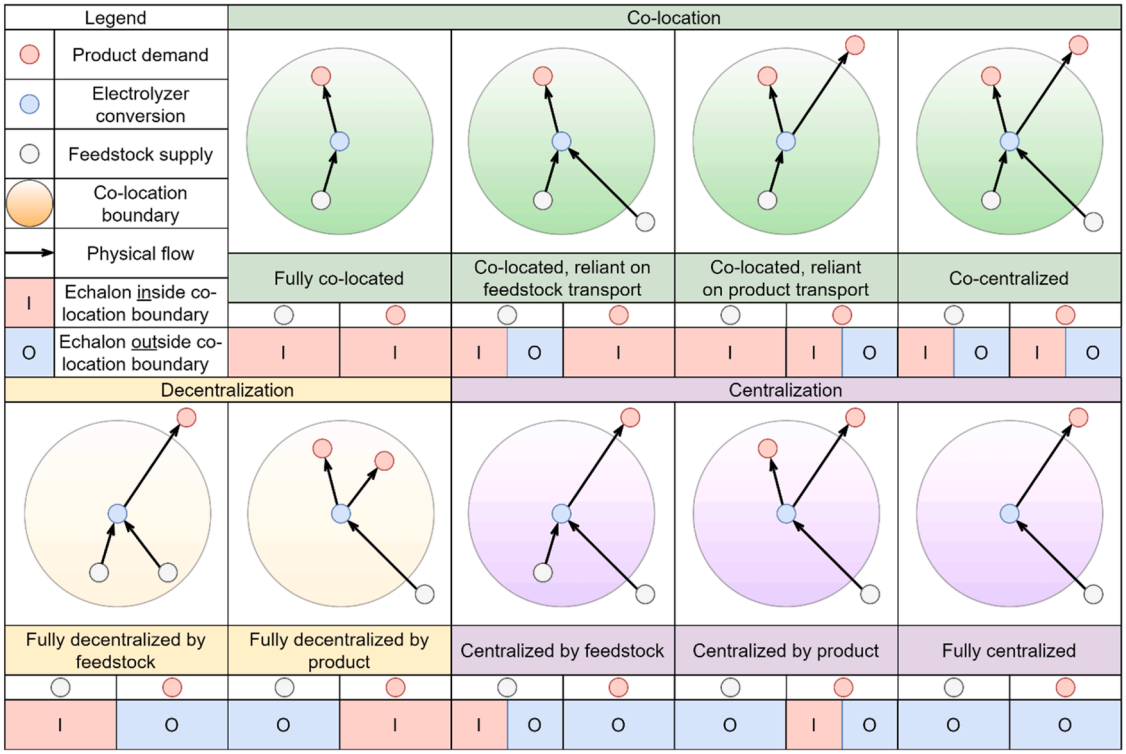

Fig. 6. Characterization of the supply chain configuration types derived from three main types: co-location, decentralization, and centralization. The location of the electrolysis plant relative to the first (CO_2 sources) and last (syngas consumption) echelons determines the configuration type.

cost of syngas production (LCOSG) as the objective function: (i) the electrolysis plant location, (ii) the size of the CO_2 electrolysis plant, (iii) the connections between the source, demand, and plant, and (iv) the size of these connections.

5.1. Supply chain formulation

Throughout the mathematical formulation, sets are written in a calligraphy font, variables are represented in lowercase italics, and parameters are capitalized in italics. The domain of a variable is displayed in italic subscript, while the roman superscript provides additional details about the symbols used in the model.

The direction of the flow of CO_2 through the SC is fixed and always follows a predefined order of SC elements, as defined in Fig. 7. The CO_2 sources in set $\mathscr{C}$ are either part of a cluster (see section 4.1) and included in subset $\mathscr{C}^{\mathrm{Eh}}$ or identified as individual sources in subset $\mathscr{C}^{\mathrm{Ci}}$. Within the clustered sources $\mathscr{C}^{\mathrm{Eh}}$, the CO_2 first needs to be transported to the center location of that cluster (referred to as the 'exclusive hub'). All the exclusive hubs are part of the set $\mathscr{EH}$. This additional transport step is not required for individual sources in $\mathscr{C}^{\mathrm{Ci}}$, which are converted into the analogous set $\mathscr{C}i$ without any transport costs. From location $\mathscr{C}i$ or $\mathscr{EH}$, CO_2 can be transported directly to other locations. All the syngas demand locations are part of the set $\mathscr{S}$, while all the potential locations for the electrolysis plant are collected in set $\mathscr{E}$. This set is built up of the locations of set $\mathscr{EH}$, $\mathscr{C}i$, $\mathscr{S}$ and a grid of center points of the NUTS-2 regions. The set $\mathscr{X}$ (not included in Fig. 7) compiles the CAPEX, OPEX, and total expenditures of all SC echelons.

5.2. Mass balance equations

5.2.1. Capture

The capture technology used for each CO_2 source is indexed using the set $\mathscr{T}c$. From the available CO_2 sources ($CO2^{\mathrm{In}}_{c,tc}$), a fraction (cap^{Fr}_{c}) enters the supply chain ($co_2flow^{\mathrm{Cap}}_{c}$). Where in Eq. (1),

$$\mathrm{eqCO2}^{\mathrm{In}}_{c},\ \sum_{tc} CO2^{\mathrm{In}}_{c,tc}\cdot cap^{\mathrm{Fr}}_{c} = co_2flow^{\mathrm{Cap}}_{c},\ \forall\ c\ \in\ \mathscr{C}. \tag{1}$$

Constraints Eq. (2) and Eq. (3) set a minimum threshold for waste and PP's capture and compression fraction. The equations are defined only when a source ($\mathscr{C}$) is part of subset $\mathscr{C}^{\mathrm{Cap}}$. cap^{Fr}_{c} regulates the fraction of CO_2 that is captured and compressed, or only compressed, from a CO_2 source. This variable can also become zero if there is no CO_2 capture from that source. Therefore, the binary variable cap^{Bound}_{c} is introduced to turn cap^{Fr}_{c} into a semi-continuous variable. The scalars that define the capture fraction bounds are FR^{Low} and FR^{Up}. We define the lower capture fraction via

$$\mathrm{eqCapture}^{\mathrm{Min}}_{c},\ cap^{\mathrm{Fr}}_{c} \geq FR^{\mathrm{low}}\cdot cap^{\mathrm{Bound}}_{c},\ \forall\ c\ \in\ \mathscr{C}^{\mathrm{Cap}}. \tag{2}$$

Analogous the upper limit of the capture fraction is defined via

$$\mathrm{eqCapture}^{\mathrm{Max}}_{c},\ cap^{\mathrm{Fr}}_{c} \leq FR^{\mathrm{up}}\cdot cap^{\mathrm{Bound}}_{c},\ \forall\ c\ \in\ \mathscr{C}^{\mathrm{Cap}}. \tag{3}$$

Eq. (4) applies to the CO_2 sources that are captured and compressed or only compressed. This ensures that the capture fraction (cap^{Fr}_{c}) is below the specified maximum capture fraction (FR^{All}). We define

$$\mathrm{eqCapFr}^{\mathrm{Max}}_{c},\ cap^{\mathrm{Fr}}_{c} \leq FR^{\mathrm{All}},\ \forall\ c\ \in\ \mathscr{C}. \tag{4}$$

5.2.2. CO_2 transport

$co_2flow_{c*,\,c*}$ is a decision variable that determines the flow between different echelons in the SC. The $_{c*,\,c*}$ index here is a placeholder for the (sub)sets related to capture and conversion (e.g., $\mathscr{C}^{\mathrm{Ci}}$, $\mathscr{C}i$, $\mathscr{C}^{\mathrm{Eh}}$, $\mathscr{EH}$, or $\mathscr{E}$). $\mathscr{P}^{\mathrm{Eh}}$ and $\mathscr{P}^{\mathrm{Ci}}$ are predefined sets which are the Cartesian product of $\mathscr{C}^{\mathrm{Eh}} \times \mathscr{EH}$ and $\mathscr{C}^{\mathrm{Ci}} \times \mathscr{C}i$ respectively. These sets enable the distinction between exclusive hubs and individual sources. The transport from the captured CO_2 to the exclusive hub is defined in constraint (5), also called

$$\mathrm{eqEH}_{ceh},\ co_2flow^{\mathrm{Cap}}_{ceh} = \sum_{eh} co_2flow_{ceh,eh}\cdot\mathscr{P}^{\mathrm{Eh}}_{ceh,eh},\ \forall\ ceh\ \in\ \mathscr{C}^{\mathrm{Eh}}. \tag{5}$$

Eq. (6) describes the flow from the exclusive hub to the CO_2 electrolysis plant,

$$\mathrm{eqEHE}_{eh},\ \sum_{ceh} co_2flow_{ceh,eh}\cdot\mathscr{P}^{\mathrm{Eh}}_{ceh,eh} = \sum_{e} co_2flow_{eh,e},\ \forall\ eh\ \in\ \mathscr{EH}. \tag{6}$$

The same formulation used for sources that are part of exclusive hubs (in Eqs. (5) and (6)) is used to describe the flow from the individual CO_2 source to the CO_2 electrolysis plant in Eqs. (7) and (8). We define Eq. (7) as

$$\mathrm{eqCI}_{cci},\ \mathrm{co}_2flow^{\mathrm{Cap}}_{cci} = \sum_{ci} \mathrm{co}_2flow_{cci,ci}\cdot\mathscr{P}^{\mathrm{Ci}}_{cci,\ c},\ \forall\ cci\ \in\ \mathscr{C}^{\mathrm{Ci}}, \tag{7}$$

and Eq. (8) as

$$\mathrm{eqCIE}_{ci},\ \sum_{cci} co_2flow_{cci,ci}\cdot\mathscr{P}^{\mathrm{Ci}}_{cci,\ c} = \sum_{e} co_2flow_{ci,e},\ \forall\ ci\ \in\ \mathscr{C}i. \tag{8}$$

5.2.3. Syngas transport

In Eq. (9), the CO_2 that enters into the CO_2 electrolysis plant is converted into syngas using a stoichiometric conversion factor CO^{Conv}_{2} of 0.73, which is calculated in SI 8. CO^{Y}_{2} determines the efficiency of CO_2 conversion into syngas. We introduce

$$\mathrm{eqES}_{e},\ \left(\sum_{eh} co_2flow_{eh,e} + \sum_{ci} co_2flow_{ci,e}\right)\cdot CO^{\mathrm{Conv}}_{2}\cdot CO^{\mathrm{Y}}_{2} = \sum_{s} sgflow_{e,s},\ \forall\ e\ \in\ \mathscr{E}. \tag{9}$$

$sgflow_{e,s}$ is the resulting flow of syngas that is transported from the CO_2 electrolysis plant to the demand location. Note that only the conversion into syngas is considered in the mass balance. Other inputs and side streams, like water, are assumed to be readily available, while oxygen and unreacted CO_2 are vented and not further considered.

5.2.4. Syngas demand fulfillment

Eq. (10) ensures that the maximum size of the CO_2 electrolysis plant is capped via the maximum syngas flow at 1 Mtonne syngas/year based on the current European upper-scale value of the syngas demand. So that

$$\mathrm{eqMax}^{\mathrm{Flow}}_{e},\ \sum_{s} sgflow_{e,s} \leq 1,\ \forall\ e\ \in\ \mathscr{E}. \tag{10}$$

In the base scenario, the syngas flow to a demand site cannot exceed its predefined demand. Since we set Eq. (11)

$$\mathrm{eqDemand}^{\mathrm{Flow}}_{s},\ \sum_{e} sgflow_{e,s} \leq SG^{\mathrm{Demand}}_{s},\ \forall\ s\ \in\ \mathscr{S}. \tag{11}$$

SG^{Demand}_{s} is specific for each location and set to 1 in the SGD1 scenario. The effect of the system's syngas demand on the SC configuration is investigated via Eq. (12) by changing the input parameter MRK^{Fr}. MRK^{Fr} is a fraction of the total European syngas market and ranges from 0.001 (corresponding to 13.9 ktonne syngas/year) to 1 (13.9 Mtonne syngas/year) in

$$\mathrm{eqMrk}^{\mathrm{Fulfill}},\ \sum_{e,s} sgflow_{e,s} = MRK^{\mathrm{Fulfill}}\cdot MRK^{\mathrm{Fr}}. \tag{12}$$

5.3. Cost equations

5.3.1. Capture cost

Carbon dioxide from PP and waste was assumed to be captured using an amine-based post-combustion technology. The CO_2 stream was conditioned and compressed to a supercritical state to meet pipeline

requirements (150 bar). The model developed by Hasan et al. (2012) was used and adjusted to fit the case context:

(i) A conversion factor was used to convert the CO_2 stream flow from Mtonne/year into mol/s based on a pre-defined flue gas composition for each source (see SI 3 and 4).
(ii) Currency and year change from $\$_{2009}$ to EUR_{2018} (see SI 5).
(iii) The capital recovery factor (CRF) was adjusted from 0.154 to 0.10 (based on a lifetime of 20 years and 8 % interest).
(iv) In Hasan et al. (2012), the electricity cost of CO_2 capture was included in the OPEX cost function. A disaggregated cost function was not presented; therefore, the electricity price could not be changed without assuming a percentage of electricity contribution to the OPEX. It was assumed that 21 % of the capture OPEX was attributed to the electricity consumption (Wang et al., 2023).

For CO_2 compression, using the method described in McCollum and Ogden (2006), the CO_2 was compressed to 150 bar, and the costs were converted from $\$_{2005}$ to EUR_{2018} (see SI 5).

Eqs. (13) and (14) describe the capture cost and flow of the CO_2 stream entering the SC. The factor λ is defined as a continuous positive variable for the interpolation of the piecewise linear segments. λ is present in the cost (13) and flow Eq. (14) and links the captured CO_2 flow ($co_2flow_c^{\mathrm{Cap}}$) with the total capture cost (annualized CAPEX and OPEX, $cap_{c,x}^{\mathrm{Cost}}$). In the cost equation, the interpolation factor is multiplied by $CC_{tc,\,"\mathrm{cost}",q}^{\mathrm{Pwl}}$ that refers to the different sources, and the cost break points $\mathscr{C}$ at different segments $\mathscr{K}$. $CC_{tc,\,"flow",q}^{Pwl}$ represents the flow on the x-axis in a cost function, while $CC_{tc,\,"\mathrm{cost}",q}^{Pwl}$ represents the cost on the y-axis. The specific formulation for the piecewise-linear approximation can be found in Appendix II. $\mathscr{P}^{\mathrm{Cc}}$ is the Cartesian product between set $\mathscr{C}$ and $\mathscr{T}_c$ that serves as the link between the CO_2 source and capture/compression cost function used. We calculate the cost of CO_2 capture using

$$\mathrm{eqCost}_c^{\mathrm{CC}},\ cap_{c,x}^{\mathrm{Cost}} = \sum_{tc,q} \lambda_{tc,c,q}^{Cc} \cdot CC_{tc,\,"\mathrm{cost}",q}^{\mathrm{Pwl}} \cdot \mathscr{P}_{c,tc}^{\mathrm{Cc}}\ \forall\ c \in \mathscr{C}. \tag{13}$$

The flow that is linked to the costs comes from

$$\mathrm{eqFlow}_c^{\mathrm{CC}},\ co_2flow_c^{\mathrm{Cap}} = \sum_{tc,q} \lambda_{tc,c,q}^{\mathrm{Cc}} \cdot\ CC_{tc,\,"flow",q}^{\mathrm{Pwl}} \cdot \mathscr{P}_{c,tc}^{Cc}\ \forall\ c \in \mathscr{C}. \tag{14}$$

The Cartesian product $\mathscr{P}^{\mathrm{Cc}}$ is defined before the optimization when the input parameter $CO2_{c,tc}^{\mathrm{In}}$ is larger than zero. In Eq. (15), the capture costs of all sources are summed to find the total capture cost in the SC (cap^{Tot}),

$$\mathrm{eqCap}^{\mathrm{Tot}},\ \sum_{c} cap_{c,\,"total"}^{\mathrm{Cost}} = cap^{\mathrm{Tot}}. \tag{15}$$

5.3.2. Transport cost

Using data from the CO_2 transport simulations of the National Energy Technology Laboratory (2023), the annualized CAPEX and OPEX were calculated over the project's lifetime of 30 years and annualized using a CRF of 0.089 based on an interest rate of 8 %. The total transport cost was calculated as a sum of the annualized CAPEX and OPEX based on McCoy and Rubin (2008).

Several other minor changes were implemented to the NETL CO_2 transport cost model (2023):

(i) Location-dependent factors adjusted the American (Gulf Coast) model for the European context. These adjustments accounted for higher general labor costs (+36 %), increased labor costs due to lower productivity (+25 %), and higher material/equipment prices (+1 %) (IEAGHG, 2018; van der Spek et al., 2019).
(ii) Currency and equipment cost adjustments were made using the Chemical Engineering Plant Cost Indices (CEPCI) and the exchange rate 2018 (Eurostat, 2024b) to express all costs in EUR_{2018}.
(iii) The option to install pumps was implemented only for paths longer than 100 km to compensate for the pressure losses and keep CO_2 in the supercritical phase (Knoope et al., 2014b).

Carbon dioxide was assumed to be transported in the supercritical phase. In contrast, syngas was assumed to be transported in the gaseous phase with an average pressure of 55 bar and a H_2/CO ratio of 2. This pressure was similar to the pressure for transporting hydrogen (between 40 and 70 bar) (Weber and Perrin, 2008). Since syngas was transported in the gas phase, the method for calculating the pipeline diameter was adjusted to be based on gas phase flow (compressible fluid) instead of supercritical flow (incompressible fluid).

The same methodology to implement the piecewise linearization of capture (Eqs. (13) and (14)) is applied for transport in Eqs. (16) - (18). The $_{t^*,\ t^*}$ index here is a set placeholder for gas transport that connects the different echelons through transport connections (e.g., $\mathscr{C}^{\mathrm{Eh}}$, $\mathscr{E}\mathscr{h}\vee\mathscr{C}i$, $\mathscr{E}\vee\mathscr{E}\mathscr{h}$, $\mathscr{E}\vee\mathscr{E}$, $\mathscr{S}$). When CO_2 is transported (designated with the $_{\mathrm{CO2}^*}$, $_{\mathrm{CO2}^*}$ placeholder) Eq. (17) is valid for $co_2flow_{co2^*,co2^*}$. However, when syngas is transported the equation points to $sgflow_{e,s}$. For the transport costs we define

$$\begin{aligned}&\mathrm{eqCost}_{t^*,t^*}^{\mathrm{T}},\quad t_{t^*,t^*,\ "total"}^{\mathrm{Cost}}\\ &\quad=\sum_{q}\lambda_{t^*,t^*,q}^{\mathrm{T}}\cdot T_{"\mathrm{cost}",t^*,t^*,q}^{\mathrm{Pwl}}\quad\forall\ (t^*,\ t^*)\mid\mathscr{L}_{t^*,t^*}^{\mathrm{Flow}}.\end{aligned} \tag{16}$$

While for the flow, an equation with a similar shape is introduced via

$$\begin{aligned}&\mathrm{eqFlow}_{t^*,t^*}^{\mathrm{T}},\ co_2flow_{co2^*,co2^*}\vee sgflow_{e,s}\\ &\quad=\sum_{q}\lambda_{t^*,t^*,q}^{\mathrm{T}}\cdot T_{"flow",t^*,t^*,q}^{\mathrm{Pwl}},\ \forall\ (t^*,t^*)\mid\mathscr{L}_{t^*,t^*}^{\mathrm{Flow}}.\end{aligned} \tag{17}$$

In Eq. (18), the total cost (annualized CAPEX and OPEX) of all the transport segments are summed to find t^{Tot} in EUR_{2018}/year,

$$\mathrm{eqT}^{\mathrm{Tot}},\ \sum_{t^*,t^*} t_{t^*,t^*,"total"}^{\mathrm{Cost}} = t^{\mathrm{Tot}}. \tag{18}$$

5.3.3. Electrolysis plant equations

The upscaled electrolysis plant costs of Noordende et al. (2023) in the 2030 scenario were used to determine the CAPEX of the electrolysis plant. A CRF of 0.10 was used to annualize the CAPEX. The CO_2 electrolysis plant was assumed to operate on a continuous electricity supply at a constant price. The electricity was assumed to be always available at the consumption points (i.e., connection to the electricity grid). Steam was assumed to be generated in situ by an electric boiler, which is included in the electricity consumption figures shown in Table 2.

Given the specific characteristics of scaling up a CO_2 electrolysis plant, the scale-up was assumed to occur per module in intervals of 9 MW (Noordende et al., 2023), which corresponds to a syngas flow per module ($\mathrm{MOD}^{\mathrm{Flow}}$) of 7.8 ktonne/year with the total electricity consumption of Table 2. A CO_2 input of 13.5 ktonne CO_2/year is needed to supply this 9 MW plant. Via the $\mathrm{MOD}^{\mathrm{Flow}}$ the $sgflow_{e,s}$ is linked to the number of modules per electrolysis plant (mod_e^{Nr}), in Eq. (19) called

$$\mathrm{eqElyzr}_e^{\mathrm{Mod}},\ mod_e^{\mathrm{Nr}}\cdot\mathrm{MOD}^{\mathrm{Flow}} \geq \sum_{s} sgflow_{e,s},\ \forall\ e\ \in\ \mathscr{E}. \tag{19}$$

For the electrolysis plant, the number of modules correlates with the piecewise linear investment cost (the total not annualized CAPEX,

mod_e^{Cost}) in (20) and (21). The learning rate (LR) factor in Eq. (20) can be modified to account for cost reductions due to learning; see

$$\text{eqCost}_e^{Ele},\ \ mod_e^{Cost} = \sum_q \lambda_{e,q}^{Ele} \cdot EPC^{Pwl}_{"cost",q} \cdot (1 - LR),\ \forall\ e \in \mathscr{E}. \tag{20}$$

We define the equation for the number of modules via

$$\text{eqNumber}_e^{Ele},\ \ mod_e^{Nr} = \sum_q \lambda_{e,q}^{Ele} \cdot EPC^{Pwl}_{"module",q},\ \forall\ e \in \mathscr{E}. \tag{21}$$

The electricity consumption of the electrolysis plant is composed of two elements, namely, the conversion and balance of the plant. Electricity consumption factor for the conversion (E^{Conv}) is converted to cost factors per flow of syngas in the following equation,

$$\text{eqElyzr}^{Conv},\ EC^{Cost} \cdot E^{Conv} \cdot 10^6 = CONV^{Elyzr}. \tag{22}$$

The cost factor per syngas flow for the balance of the plant (E^{Bop}) is defined in Eq. (23), also named

$$\text{eqElyzr}^{Bop},\ EC^{Cost} \cdot E^{Bop} \cdot 10^6 = BOP^{Elyzr}. \tag{23}$$

$CONV^{Elyzr}$ and BOP^{Elyzr} are then used in Eq. (24) to calculate the operational electricity consumption,

$$\text{eqElyzr}_e^{Elect},\ \sum_s sgflow_{e,s} \cdot \left(CONV^{Elyzr} + BOP^{Elyzr}\right) = elyzr_e^{Elect},\ \forall\ e \in \mathscr{E}. \tag{24}$$

The total CAPEX of the electrolysis plant is estimated by mod_e^{Cost} in Eq. (20). The stacks in the plant have a shorter lifetime compared to the rest of the plant. The lifetime was assumed to be five years or 40,000 operating hours, assuming 8,000 operating hours per year for the whole SC (Detz et al., 2023). Due to their shorter lifetime (LT^{Stack}), stack replacements were considered as an OPEX ($elyzr_e^{Stack}$). The costs of stack replacements in Eq. (25) are based on (i) the standard module cost (BM^{Cost}), (ii) the learning rate (LR), (iii) the number of modules that need to be placed at a specific location (mod_e^{Nr}) and (iv) a fraction of the investment cost attributed to the stack. The stack investment cost fraction was assumed to be 0.2 of the CAPEX (which includes the stack, the balance of stack, and installation costs) based on Noordende et al. (2023). We define the stack replacement costs as

$$\text{eqElyzr}_e^{Stack},\ \frac{BM^{Cost} \cdot (1 - LR) \cdot mod_e^{Nr} \cdot FS}{LT^{Stack}} = elyzr_e^{Stack},\ \forall\ e \in \mathscr{E}. \tag{25}$$

Other OPEX includes operations and maintenance costs derived from the CAPEX part that is not associated with the stack. The O&M are based on the total investment cost and operations and maintenance factor (OM^{Use}). Note that the O&M is part of the OPEX cost function in the other echelons. The O&M refers to the balance of plant fraction since the stack replacements are considered separately (Eq. (25)). Therefore, Eq. (26) is defined as follows,

$$\text{eqElyzr}_e^{OM},\ mod_e^{Cost} \cdot (1 - FS) \cdot OM^{Use} = elyzr_e^{OM},\ \forall\ e \in \mathscr{E}. \tag{26}$$

In Eq. (27), the yearly OPEX of the electrolyzer is calculated by summing the stack replacement cost, O&M, and electricity costs,

$$eqElyzr_e^{OPEX},\ elyzr_e^{Stack} + elyzr_e^{OM} + elyzr_e^{Stack} = elyzr^{Cost}_{e,"opex"},\ \forall\ e \in \mathscr{E}. \tag{27}$$

The non-stack fraction of the total CAPEX is annualized in Eq. (28) by using the capital recovery factor of the plant. We set

$$\text{eqElyzr}_e^{CAPEX},\ mod_e^{Cost} \cdot \text{CRF}^{Plant} \cdot \text{FS} = \text{elyzr}^{Cost}_{e,"capex"},\ \forall\ e \in \mathscr{E}. \tag{28}$$

The total electrolyzer costs are calculated by summing the annualized CAPEX and OPEX in Eq. (29)

$$\text{eqElyzr}^{Tot},\ elyzr^{Tot} = \sum_{e,x} elyzr^{Cost}_{e,x}. \tag{29}$$

5.3.4. Total annualized supply chain costs

The $totsc^{Cost}$ of Eq. (30) comprises the annualized CO_2 capture (cap^{Tot}), gas transport t^{Tot} (which comprises ceh^{Tot}, cie^{Tot}, ehe^{Tot} and es^{Tot}), and CO_2 conversion cost ($elyzr^{Tot}$),

$$\text{eqTotal},\ ceh^{Tot} + cie^{Tot} + ehe^{Tot} + es^{Tot} + cap^{Tot} + elyzr^{Tot} = totsc^{Cost}. \tag{30}$$

5.3.5. Objective function

The cost variables are optimized to identify the SC configurations with the lowest LCOSG via

$$\text{eqLCOSG},\ \frac{totsc^{Cost}}{MRK^{Fulfill} \cdot MRK^{Fr}} \cdot 10^6 = lcosg. \tag{31}$$

This is achieved by minimizing the annualized cost variable ($totsc^{Cost}$), subject to a fixed syngas target parameter:

$$\underset{\text{Variable: binary, integer, and continuous}}{\textit{Minimize}\quad \{\ lcosg\ \}}$$

Subject to Eqs. (1)-(31).

The mathematical model is in a steady state, and the SC configuration remains constant over the lifetime. The decision variables are not indexed over time. The investment for the whole SC is made in year 1.

6. Results and discussion

6.1. Model performance

In total, seven different scenarios (Table 3) were optimized for different market penetrations (26 different MRK^{Fr}) ranging from 0.1 to 100 percent. The model contains 2,109,712 equations, 2,717,620 variables, and 787,761 discrete variables. The model was implemented in GAMS (General Algebraic Modeling System) (version 44.4.0) and solved with Gurobi (10.0.2) using the DelftBlue supercomputer (Delft High Performance Computing Centre (DHPC), 2022). Here it ran on 48 cores with 192 GB of memory available. The model continued to the next MRK^{Fr} if the optimality tolerance of 0.02 % was reached or if a six-hour time limit was reached. For more details about the optimality gap, see Appendix III.

6.2. The case under the base scenario

Fig. 8A displays the CO_2 origin of the syngas SC in the base scenario. Syngas market fulfillments lower than 2 % were generally fulfilled using CO_2 from bioethanol plants. At syngas demands greater than 2 %, waste incineration was the dominant CO_2 source in the mix. At 25 % market fulfillment, pulp and paper started contributing to the CO_2 mix. However, waste remained the dominant CO_2 source throughout all subsequent market fulfillments. A relative decrease in the total bioethanol contribution was observed in the share, but the same sources are utilized in higher market fulfillment configurations. Despite lower capture costs in PP plants compared to waste, the longer transport distances counteracted this benefit. A syngas market size of at least 25 % was required to meet the minimum capture threshold of larger PP plants.

The model rarely selected CO_2 from biomethane plants because these sources cannot reach the scale needed for industrial syngas production. From 1077 biomethane CO_2 plants, 47 (4.4 %) could supply enough CO_2 for a 9 MW electrolyzer. Numerous separate installations would be required to reach the scale for a single module electrolyzer, which is too costly due to minimal benefits from economies of scale in compression and conversion. Small-scale CO_2 transport would require smaller pipelines than the 4-inch pipeline diameter threshold or gas phase transport, which were not included options in the model. A different SC configuration would be required to utilize the CO_2 stream from biogas, for instance, with smaller electrolyzers (0.5–7.5 MW) that operate independently of pipeline networks.

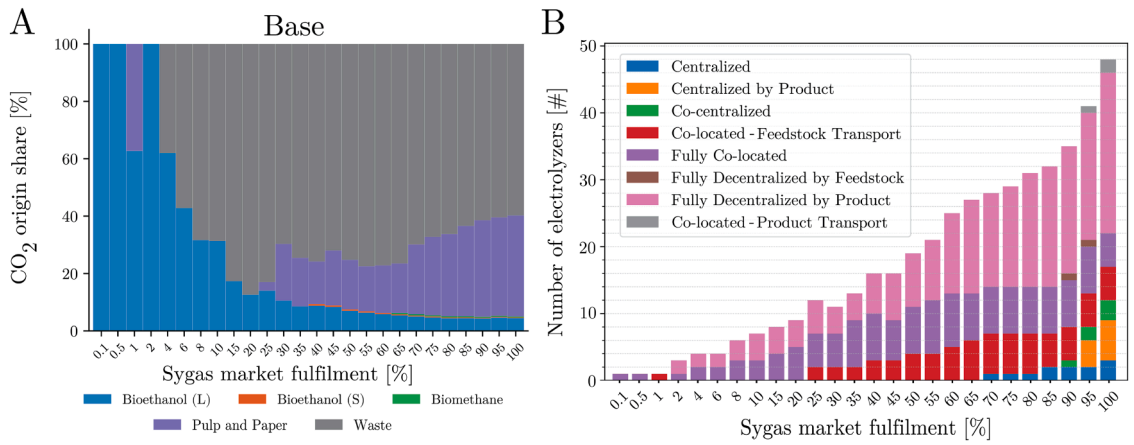

Fig. 8. A – CO_2 source mix in the base case over different market fulfilments. B – Supply chain configuration types across different market fulfilments for the base case.

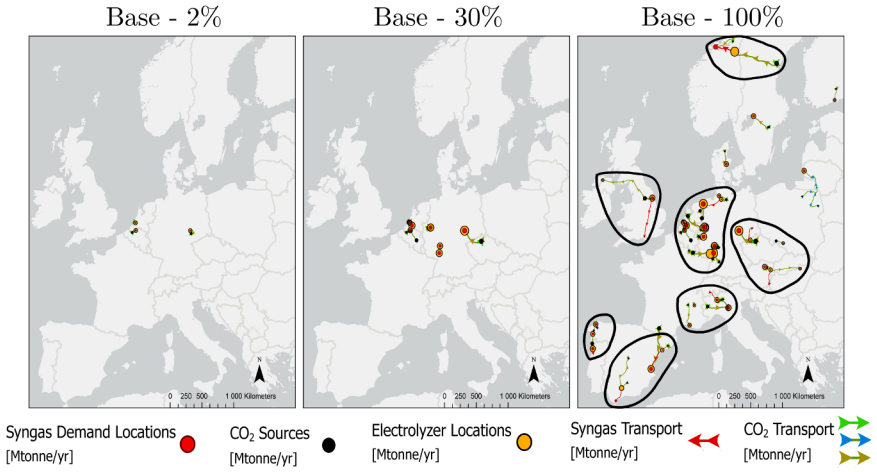

Fig. 9. Visualization of the supply chain configurations at 2 %, 30 %, and 100 % market fulfillment for the base scenario. The boundaries drawn at 100 % market fulfillment indicate potential geographic areas with clusters of CO_2 electrolysis plants.

Fig. 8B shows the selected supply chain configurations for different syngas fulfilments and different numbers of electrolyzers installed. When syngas demand fulfillment was below 25 %, the preferred SC configurations were co-located and decentralized at the product demand. Between 25 % and 65 %, feedstock transport with co-location became the third most frequently used configuration. At a market fulfillment above 70 %, fully centralized electrolyzer placements emerged. Particularly, centralized by product configurations were observed in about 30 % of electrolysis plants at full market fulfillment. In this setup, a large-scale electrolyzer was paired with CO_2 transport and on-site syngas utilization, with a small portion of syngas export. This behavior was visualized in the SC configuration maps in Fig. 9. At full market fulfillment, more than 85 % of syngas transport instances involved a size of less than 80 ktonne syngas/year. Additionally, five of the twenty-two transport connections involved flows with less than five ktonnes syngas per year. This suggests that these small-scale syngas flows were necessary to meet the demand precisely. Consequently, it can be argued that, under the input conditions of the case study, syngas transport had a niche role in the supply chain design and was used mainly under two conditions: (i) at market fulfillment above 70 %, and (ii) for syngas flows below the threshold where the CO_2 electrolysis plant reaches full economies of scale (i.e., 90 MW or 78 ktonnes of syngas per year).

To further analyze the results, the syngas demand values of 2 %, 30 %, and 100 % were selected. From Fig. 9, the first electrolyzers were placed in Benelux and Germany at a low market fulfillment. At 30 % syngas demand, the infrastructure in the Benelux was expanded, and more electrolysis plants were put in German chemical clusters. In these areas, the SCs with the lowest LCOSG were found. At 100 %, these initial infrastructures were developed further, clearly forming the most concentrated area for CO_2 electrolysis. In total, seven geographic areas with clusters of CO_2 electrolysis infrastructure were found:

1. Benelux with the chemical clusters of Ludwigshafen and the Ruhr area in Germany
2. Central Europe
3. Spain
4. Western Spain and Northern Portugal
5. UK
6. Swiss, Northern Italy, and Southern France
7. Norway and Sweden

These regions could serve as a foundation for future work, where more localized case studies can be developed based on the insights

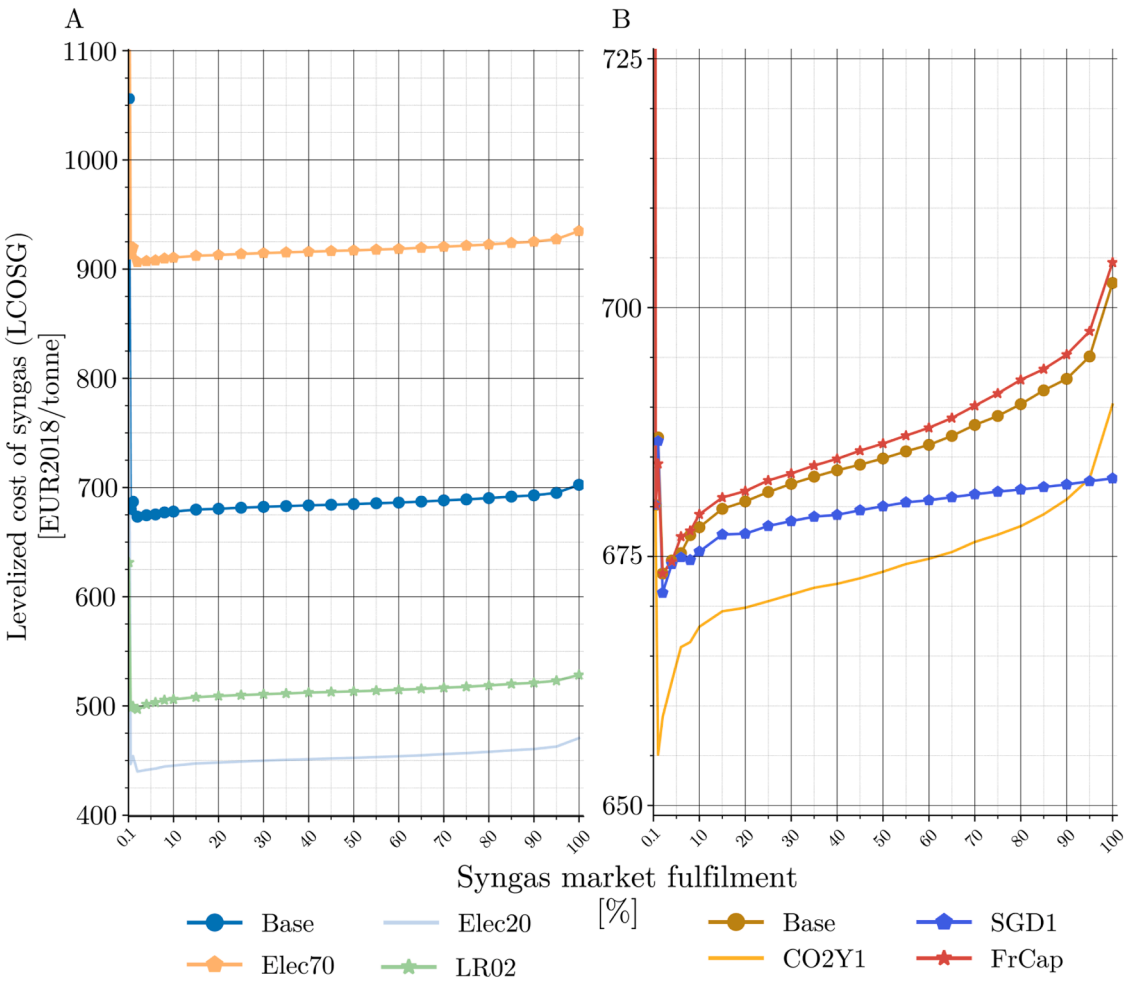

Fig. 10. The levelized cost of syngas for the different scenarios; note the difference in axis ranges between the two plots.

gained from a broad geographic analysis.

6.3. Objective function and supply chain costs for the different scenarios

6.3.1. Objective function

Fig. 10 provides an overview of the objective function (LCOSG) across different market fulfillments and scenarios. Detz et al. (2023) estimated the reference price of the fossil syngas based on the natural gas and methanol price in a range of 172–435 EUR_{2018}/tonne syngas. In their 2023 assessment of syngas production via HT CO_2E, they reported an LCOSG of 1925 EUR_{2018}/tonne syngas. Their reference system had a capacity of one ktonne of syngas per year, operating 4000 full load hours in a 2020 scenario. However, in a 2040 scenario, they estimated an LCOSG of 615 EUR_{2018}/tonne syngas due to learning and scaling effects — that is in the same order of magnitude as found in this work, using current data on prices, but considering projected 2030 electrolyzer costs.

Fig. 10A presents the scenarios with the largest impact on the LCOSG, namely the investment cost of the electrolyzer (LR02) and the electricity price (Elec20 and Elec70). The first point in the graph is at 0.1 % market fulfillment. The LCOSG lines across different scenarios behaved similarly to the change in market satisfaction. A minimum LCOSG was found at 2 % market fulfillment in the base case of 673 EUR_{2018}/tonne syngas, which is between 1.5 and 4 times higher than the fossil reference. At market fulfillment larger than 2 % an increase in cost was noted. An investment cost reduction in the electrolyzer of 80 % resulted in a 26 % LCOSG reduction. Fig. 10B presents the levelized cost of the non-cost-based scenarios. The scenario in which the availability of CO_2 was affected by a smaller capture fraction (FrCap) has a comparable LCOSG to the base scenario. The difference in LCOSG was below 1 %, indicating that capture efficiency variations barely affected the overall production costs. This negligible impact suggests that improving capture efficiency alone would not significantly reduce costs. Alternatively, increasing the CO_2 conversion efficiency in the CO_2Y1 scenario resulted in significantly lower LCOSG. Below 10 % syngas market fulfillment, the CO_2 from bioethanol could be used and supply a greater demand since more syngas could be produced with the same amount of CO_2. This resulted in fewer transport links and necessary CO_2 sources, resulting in a production cost reduction of 4.6 % at a market fulfillment of 2 %.

The SGD1 scenario showed a slower increase in the LCOSG when fulfilling larger syngas markets. In this scenario, CO_2 sources could be better matched with demand locations due to relaxed demand constraints (i.e., syngas demand in favorable locations is not capped by its identified demand). Therefore, less transport was required to use the available CO_2 sources near the demand points optimally. Furthermore, the SC configuration benefitted more from the economies of scale in capture and compression.

Finally, all the scenarios showed an increase in cost at 100 % market fulfillment, which was explained by two main factors. (i) To supply the smallest syngas demands (below 50 ktonne syngas/year), there was a trade-off between using a large electrolyzer that maximizes economies of scale and the cost of transporting expensive syngas. On the other hand, installing multiple smaller electrolyzers meant less benefit from economies of scale while it prevents syngas transport. (ii) An additional module was required in specific locations, which was partly utilized to meet demand. This effect could have been reduced when the individual

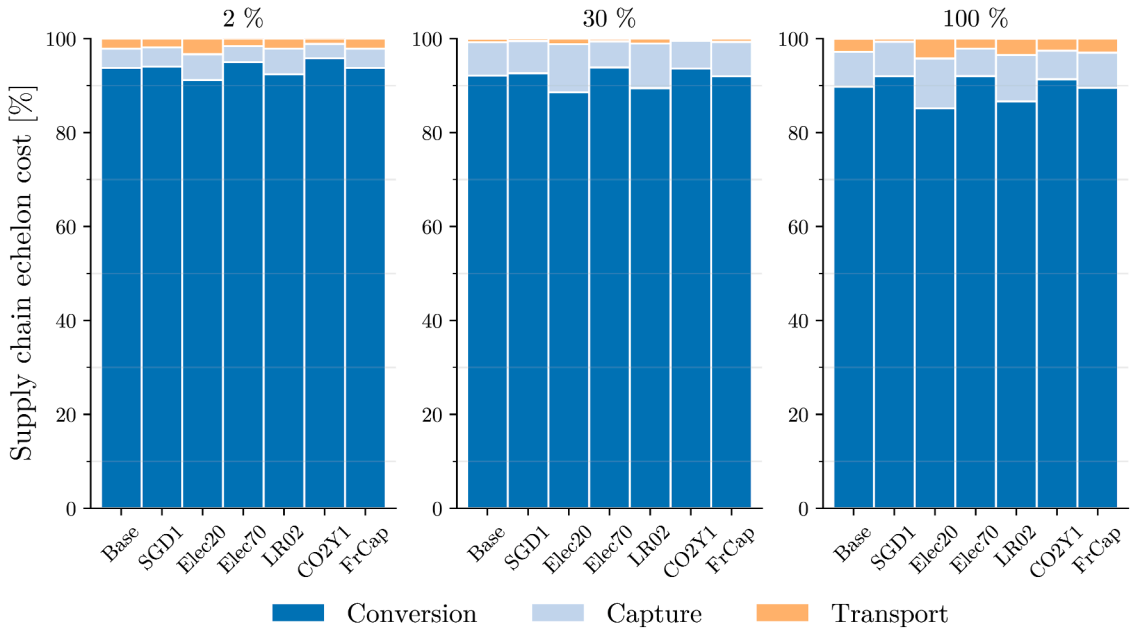

Fig. 11. The levelized cost of syngas contribution of the supply chain stages for different scenarios over different syngas market fulfillments, 2, 30, and 100 %, respectively.

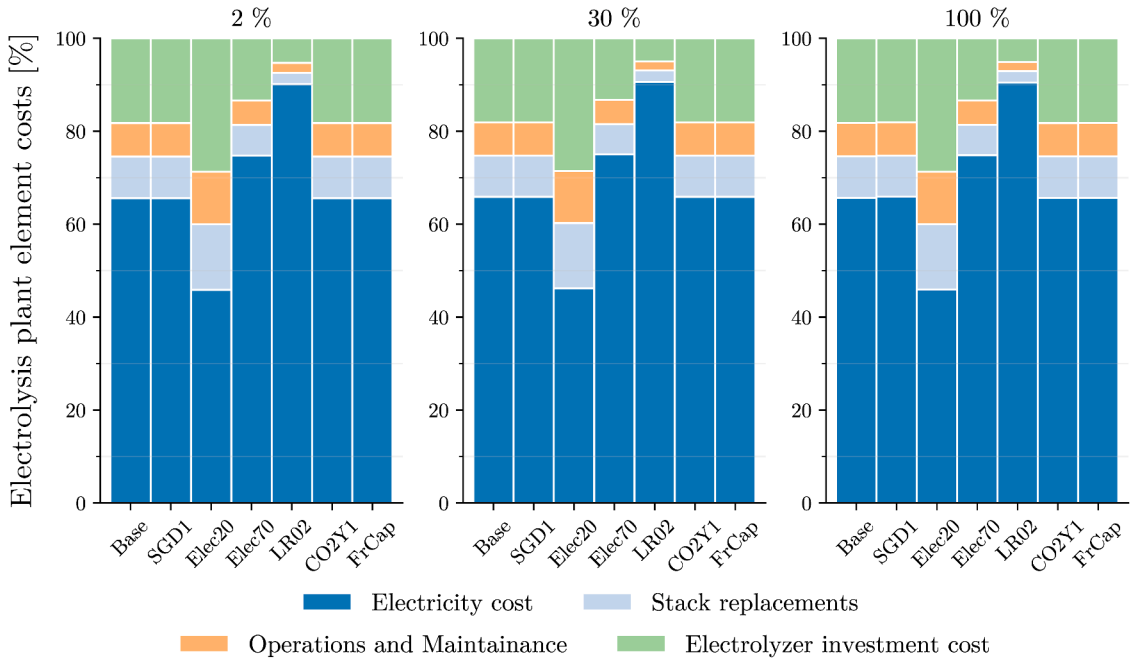

Fig. 12. Relative contribution of the electrolysis plant elements over different syngas market fulfillments, 2, 30, and 100 %, respectively.

module sizes were allowed to be smaller, resulting in better matching and lower LCOSG.

6.3.2. *Cost contribution of supply chain elements to the levelized cost of syngas*

The electrolyzer contributed significantly to the SC cost; see Fig. 11. At 2 % demand fulfillment, the electrolyzer had an average relative contribution of over 90 %. When the market fulfillment reached 100 %, the average contribution of transport to the LCOSG was only 3 %. However, in the SGD1 scenario, the average contribution of transport to the cost across all syngas demand fulfilments was even lower, at only 0.9 %. In this scenario, the electrolysis plant size matched the local availability of CO_2, reducing the need for transport. The capture or compression contribution was larger at a market fulfillment of 30 %. A wider variety of CO_2 sources was required to fulfill the demand, which was more expensive than the compression of CO_2 from the bioethanol plant at the 2 % market fulfillment.

6.3.3. *Cost contribution of electrolyzer elements*

Fig. 12 presents the contribution to the LCOSG of the specific elements in the electrolyzer (i.e., electricity, O&M, stack replacement, and annualized total installed cost of the electrolyzer). Electricity had the largest contribution, as also observed by Detz et al. (2023) in their 2040 scenario. Before 2040, the CAPEX was the dominant factor in the LCOSG

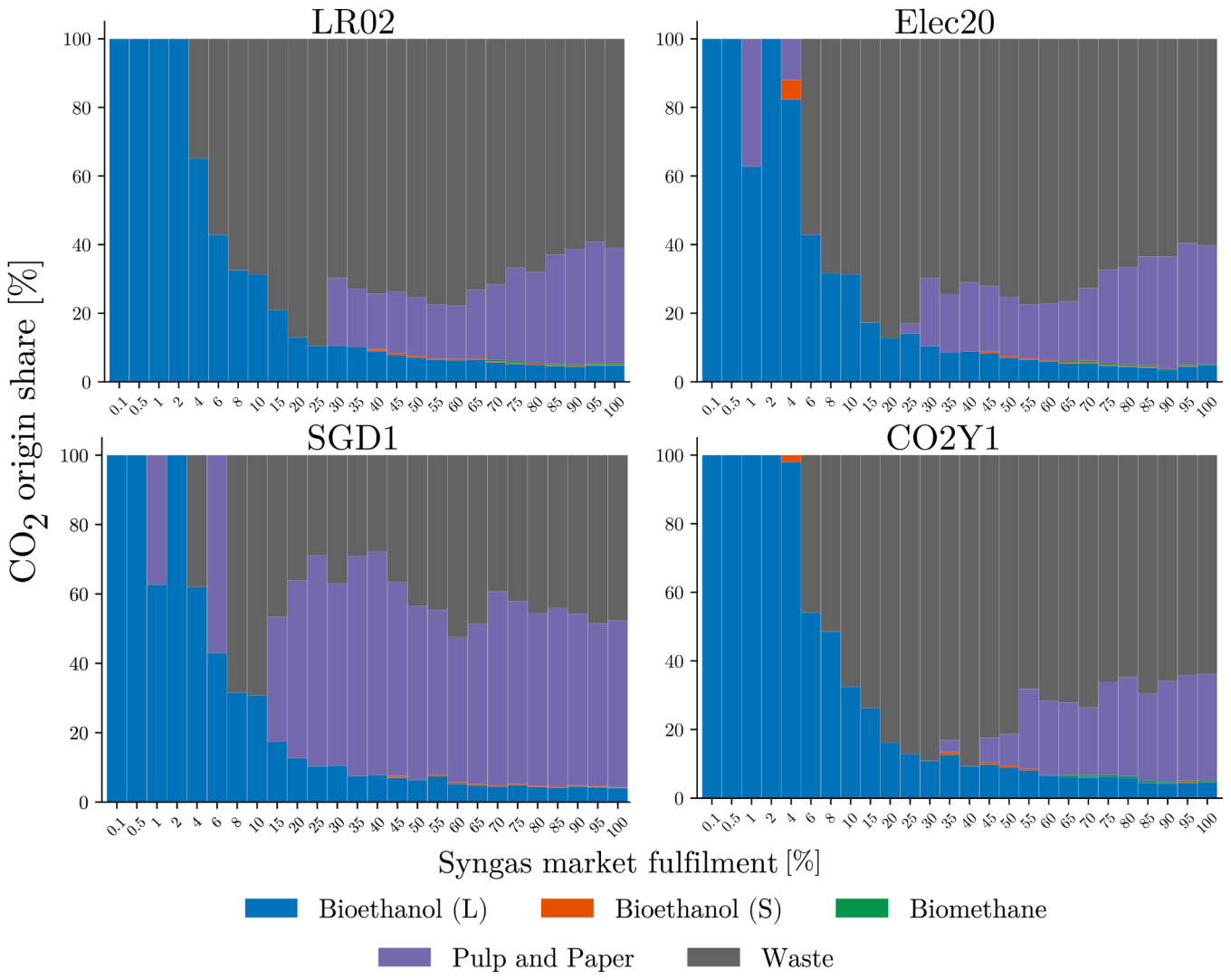

Fig. 13. CO_2 origin in the supply chain configurations for different scenarios, LR02, Elec20, SGD1, and CO_2Y1.

since major CAPEX reductions due to learning, manufacturing improvements, and economies of scale had yet to take place.

After 2 % market fulfillment in the base scenario, 66 % of the electrolyzer cost was attributed to electricity consumption. Investment cost and electricity price changes strongly impacted the relative distribution of the electrolysis plant elements, as seen from the Elec20,

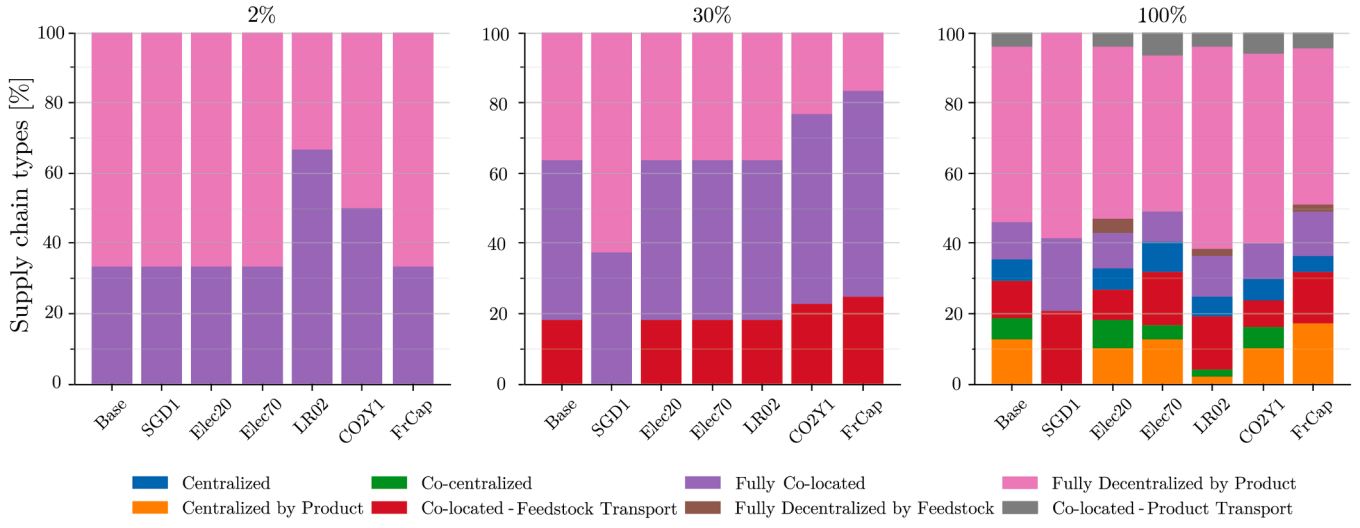

Fig. 14. Supply chain configurations for all the scenarios for different syngas market fulfillments, 2, 30, and 100 %, respectively.

Elec70, and LR02. No significant change was observed in the contribution of the cost elements for the electrolysis plant beyond the 2 % syngas market fulfillment. At this point, the CO_2 electrolysis plants were fully upscaled. Increasing the syngas market fulfillment beyond 2 % did not yield additional benefits from economies of scale in the conversion process. Consequently, this led to the same distribution of cost categories.

6.4. Supply chain configurations for all the scenarios

6.4.1. CO_2 sources used

When comparing the CO_2 sources used in the SGD1 scenario from

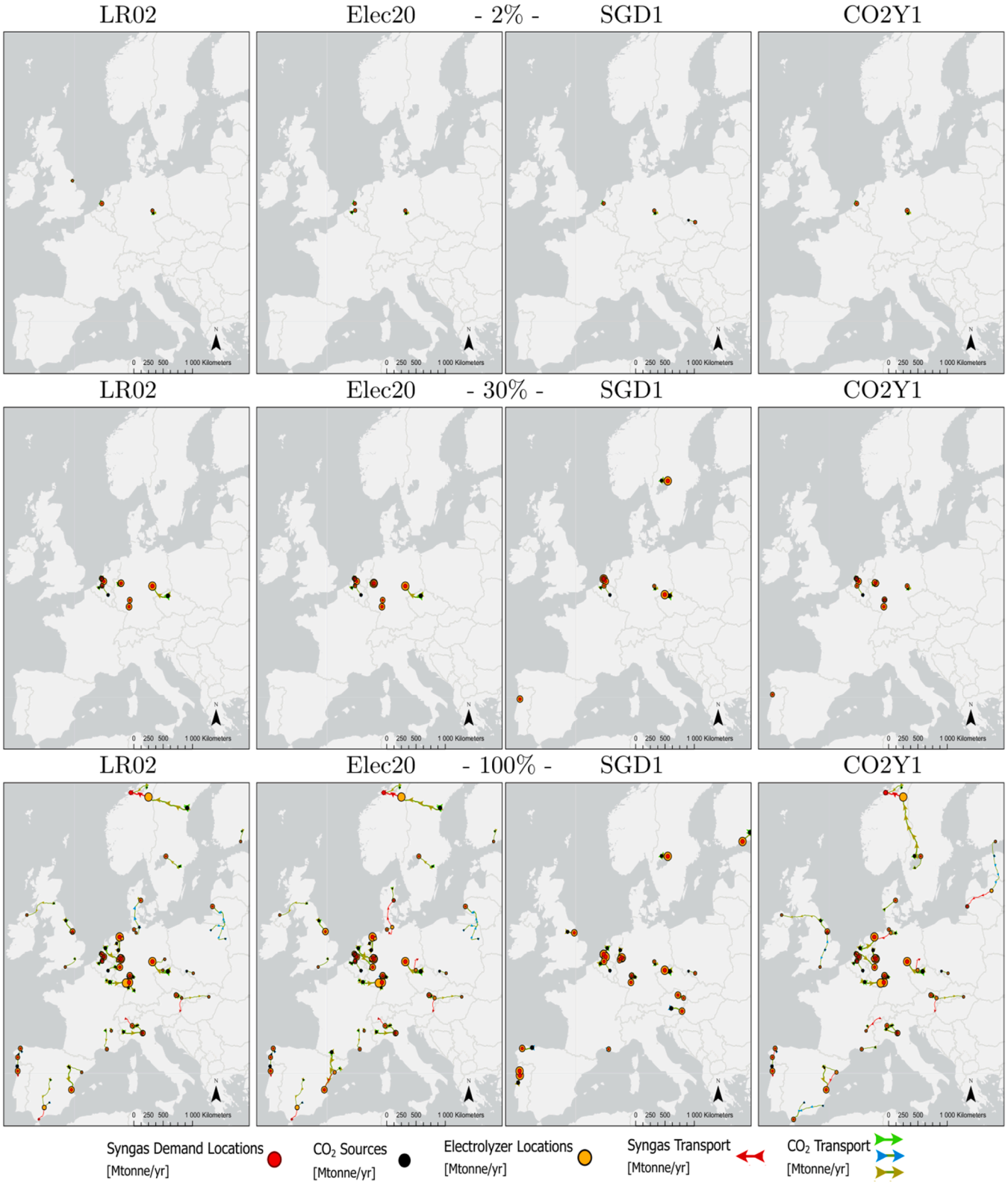

Figure 15. Visualization of the supply chain configurations at 2 %, 30 %, and 100 % market fulfillment for the LR02, Elec20, SGD1, and CO_2Y1 scenarios.

Fig. 13 to the base scenario, pulp and paper plants played a significantly larger role. Their contribution to the CO_2 syngas mix across different levels of market fulfillment noticeably increased. With a relaxed syngas demand constraint, optimal matches were possible with the larger PP plants at a lower market fulfillment. This made PP the dominant CO_2 source in the SC. The CO_2 mix in the LR02 and Elec20 scenarios was comparable to the base scenario, with the preferred order of sources being bioethanol, waste, and pulp and paper, respectively. In the CO_2Y1 scenario, less CO_2 was required, allowing CO_2 from waste and bioethanol to fulfill a higher share of demand. Carbon dioxide from pulp and paper became less critical for meeting syngas demand. As high as 40 % of the syngas market could be supplied from waste and bioethanol CO_2 compared to the 20 % in the base scenario.

6.4.2. Supply chain types

In Fig. 14, the chosen SC configurations are presented. At 2 % market fulfillment, a typologically similar SC was found for all the scenarios. Here, the electrolyzer was fully co-located where possible and decentralized at the syngas demand location.

At 30 %, all scenarios except SGD1 were characterized by similar types. Given the increased demand for syngas, some fully co-located electrolysis plants were transformed into feedstock transport co-located plants by adding a CO_2 transport connection. The other dominant SC types, similar to the 2 % market fulfillment, were co-locating the electrolysis plant and placing the electrolyzer at the syngas demand location. The change of co-located plants into transport co-located plants observed in other scenarios did not occur in the SGD1 scenario. Since the demand in SGD1 was not constrained, the same electrolysis plant can utilize additional available CO_2 in the vicinity. There was a higher variety of SC configuration types at 100 % of the market fulfillment. Still, the decentralized by product type was the dominant SC, with an average occurrence above 50 % across all cases. Centralized by product was the most common centralized type, where syngas transport was used to another demand location. Finally, the SGD1 scenario heavily relied on the strategic placement of the electrolysis plant adapting to the local conditions. In this scenario, syngas transport was absent, cheaper CO_2 transport was preferred, and no small syngas demand needed to be met exactly.

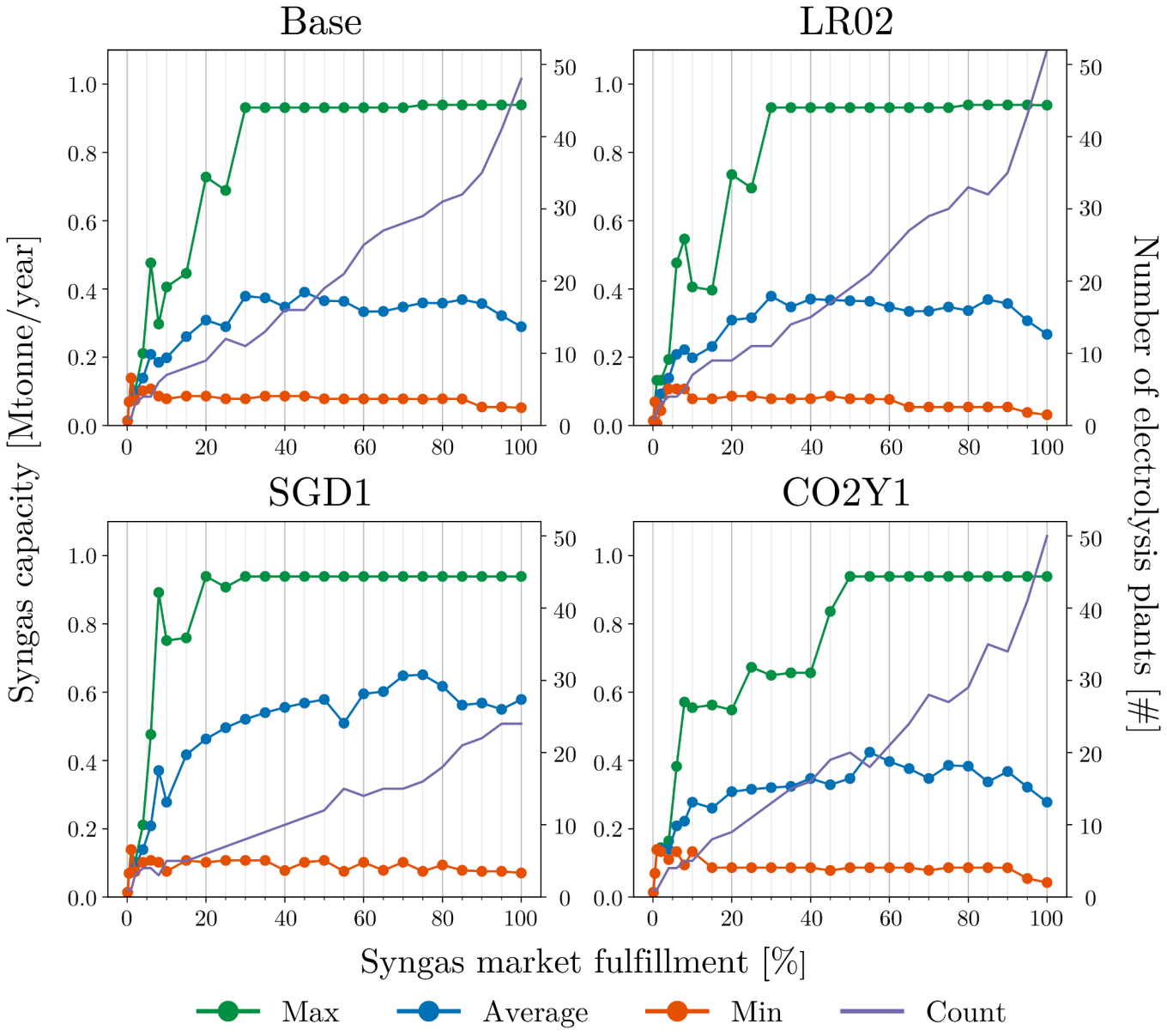

Fig. 16. Minimum, maximum, and average scale of the CO_2 electrolysis plant on the left axis and the count of electrolysis plants on the right for the Base, LR02, SGD1, and CO_2Y1 scenarios.

6.4.3. Supply chain maps

Fig. 15 presents different optimized SC configurations of the LR02, Elec20, SGD1, and CO_2Y1 scenarios. The configurations of the Elec70 and FrCap scenarios were highly comparable to that of the base scenario and are therefore presented in SI 6. At 2 % market fulfillment, the Base and Elec20 configurations were identical, and three electrolyzers were connected to bioethanol plants. Due to the increased material efficiency in the CO_2Y1 scenario, only two sources were required to provide enough CO_2 to fulfill the demand. Moreover, it explained the lower LCOSG compared to the base and SGD1 scenarios.

Fig. 15 also presents the SC configurations of the 30 % market fulfillment. Similar designs were found with demand that centers around the Netherlands, Belgium, and Germany. Finally, Fig. 15 displays the configurations for 100 % market fulfillment. The same types of configurations were found across the different scenarios. However, in the SGD1 scenario, little transport was seen, and only the most favorable electrolysis plant locations were used. Now, there are only three regions with multiple CO_2 electrolysis plants, which are (i) Benelux with the chemical clusters of Ludwigshafen and the Ruhr area in Germany, (ii) Central Europe, and (iii) Western Spain and Northern Portugal.

6.5. Electrolysis plant scale

Fig. 16 presents an overview of the syngas production capacities. The maximum size of the plants implemented by the model was 0.94 Mtonne syngas/year.

At 30 % market fulfillment, the average electrolyzer size for the Elec70, Base, LR02, and Elec20 scenarios was approximately 350 ktonne of syngas per year. The SGD1 scenario featured a 67 % larger capacity at 521 ktonne per year. In contrast, scenarios CO_2Y1 and FrCap were about 25 % lower, with syngas capacities of 260 and 278 ktonne per year, respectively. At 2 % market fulfillment, the average electrolyzer size across all scenarios was 93 ktonne of syngas per year. Except in CO_2Y1, the average size was slightly higher at 139 ktonne per year, as only two electrolysis plants were required. Even though the capacities of the electrolysis plants may be similar, the locations where the syngas demand was met might be different, see Fig. 15. Typically, the average electrolyzer size increases with increasing market fulfillment. However, after 75 % market fulfillment, the large and favorable sources were exploited, and the average size decreased again. This trend is visible in all scenarios; the size decreased when nearing complete market fulfillment since the smaller demand points had to be met. At 100 % market fulfillment, the number of electrolysis plants was slightly lower than the syngas demand locations due to plants being connected to multiple syngas demand locations. In the current analysis, the electrolyzer was connected to a continuous electricity supply. Dealing with the intermittency requires scaling the renewable electricity plant and storage options, as in Morgenthaler et al. (2020). The scale indication proposed here was limited, resulting from the CO_2 supply and syngas demand matching at an industrial scale, although different limits might emerge from the energy perspective.

7. Conclusion

The current work explored the cost-effectiveness of CO_2-based syngas supply chains installed in Europe. The goal of the supply chains was to provide syngas to the chemical industry, focusing on strategic decisions such as configuration and sizing of the electrolysis plants. The Benelux area, together with the chemical clusters of Ludwigshafen and the Ruhr area in Germany, is identified as a promising geographic area for implementing these supply chains. Using current data on biogenic CO_2 sources and syngas demands, the CO_2 electrolysis plants were preferably placed co-located or decentralized by product. In this way, only CO_2 was transported to the demand location, and the model did not select syngas transport. There was a niche application for syngas transport at flows smaller than the upscaled electrolysis plant size (i.e., 90 MW). Furthermore, the size of the electrolysis plant is determined by the syngas demand and not by the availability of CO_2.

The electrolysis plants were matched with large-scale bioethanol plants, reaching economies of scale in the conversion at the lowest CO_2 capture and compression costs. Since the availability of bioethanol in Europe is only 2.3 Mtonne CO_2 annually, the relative contribution decreases at larger syngas market fulfillments. By increasing the syngas demand fulfillment, CO_2 from waste incineration was the second option as the locations were favorably co-located to syngas demands, and the size was large enough to benefit from economies of scale in capture and transport.

At 2 % syngas market demand fulfillment, the lowest LCSOG was found at 673 EUR_{2018}/tonne, with electrolysis plants having an average size of approximately 100 ktonne syngas/year. This cost was estimated to be between 1.5 and 4 times higher than the fossil reference. At larger syngas market fulfilments, the size increased to an average of 340 ktonne syngas/year (LCSOG 685 - 705 EUR_{2018}/tonne). When the conversion scale was limited to a maximum of 1 Mtonne syngas/year, the average electrolysis plant size went up to 565 ktonne syngas/year (LCSOG 680 - 685 EUR_{2018}/tonne).

Future research should investigate the effect of renewable electricity on the size of the electrolysis plant. The availability of renewable electricity is expected to impact the number of operating hours, which in turn impacts the plant's conversion size. Furthermore, the current model allocates the total cost of new infrastructure to the CO_2E supply chain but overlooks possible synergies with CCS or other supply chains. Potentially, the LCSOG could be improved by sharing infrastructure when these supply chains are integrated. The current modeling framework provides a solid foundation to be extended into applications where CO_2E has an integrated role in a more complex system.

CRediT authorship contribution statement

Thijmen Wiltink: Writing – original draft, Visualization, Methodology, Investigation, Formal analysis, Data curation. **Andrea Ramírez:** Writing – review & editing, Supervision, Methodology, Conceptualization. **Mar Pérez-Fortes:** Writing – review & editing, Project administration, Methodology, Funding acquisition, Conceptualization.

Declaration of competing interest

The authors declare that they have no known competing financial interests or personal relationships that could have appeared to influence the work reported in this paper.

Acknowledgments

This research receives funding from the project "Addressing the multiscale challenge of CO2 electrochemical reduction", NWO ECCM tenure track grant (project number ECCM.TT.ECCM.009). The authors thank the project team members, Josephine Vos, Dr. Sanghamitra Chakravarty, and Dr. Marula Tsagkari, for all the fruitful discussions regarding CO_2 electrolysis from different perspectives, as well as Dr. Özlem Mahmutoğulları for the insightful discussions on supply chains and optimization-related topics.

Supplementary materials

Supplementary material associated with this article can be found, in the online version, at doi:10.1016/j.compchemeng.2025.109187.

Appendix I – Electrolyzer scaling

The solid oxide electrolysis plant scales up by repeating several smaller components, as visualized in Figure 17. Over 100 solid oxide electrolysis (SOE) cells are bundled together to form a stack with a typical size of up to 100 kW. This stack is then incorporated into a larger structure known as a hot-box with a capacity of 1.5 MW. Six of these hot-boxes are bundled together to form a repeating module of 9 MW. This module includes all the required supporting systems, such as power electronics, purification, and compression. Up to 10 of these modules are then arranged in a standardized way to form a system of 90 MW. Depending on the required plant size, multiple systems may be needed for applications bigger than 100 MW.

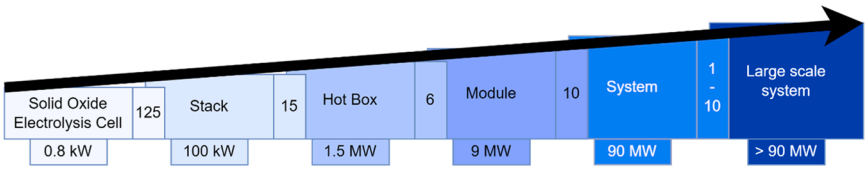

Fig. 17. Scale-up of an electrolysis plant based on the configuration and sizes of Noordende et al. (2023).

Fig. 18 visualizes the electrolyzer cost function based on the number of installed modules. It is assumed that beyond ten modules, there is no effect of scale increase, resulting in a horizontal cost per capacity line. The number of modules is an integer, starting with a single module. Between 1 and 10 modules, the CAPEX decreases with the assumed exponential scaling factor of 0.6.

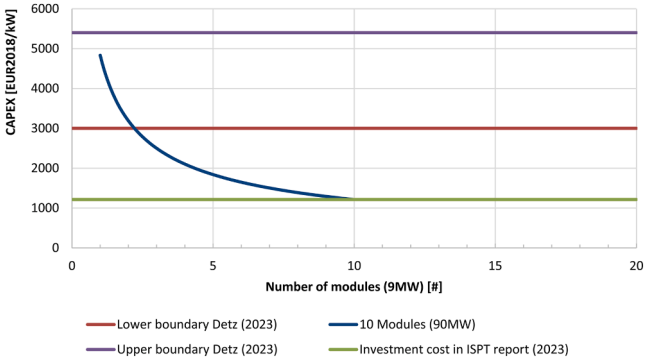

Fig. 18. Effect on the CAPEX due to the increased number of modules. The upper and lower cost boundaries are based on Detz et al. (2023).

Appendix II – Piece interpolation equations

Piece interpolation constraints

A piecewise-linear approximation is implemented via a Convex Combination formulation with a logarithmic number of binary variables; the formulation is based on the mathematical GAMS implementation of Kalvelagen (2019). This formulation is used for capture, compression, gas transport, and the electrolysis plant. The formulation is presented below as a general formulation. also, the specific formulation is provided below.

For this formulation, a Boolean incidence set I is required for linking the interpolation and binary variable, see Eq. (32). This incidence set is used to depict the connection between λ and δ. δ_b is a binary variable used for encoding the segments and designates which ones are selected.

$$\text{eqI, } \mathscr{I}_{b,\ b01,q} = \begin{cases} 1 \ - \ \textit{if breakpoint q is part of a segment k that has binary b equal to b01} \\ 0 \ - \ \textit{otherwise} \end{cases} \tag{32}$$

Eqs. (33) and (34) ensure that the segment selection and interpolation variables are linked via the opposite of the incidence matrix.

$$\text{eqLink0} \sum_{q \mid \mathit{not}\mathscr{I}_{b,\ "0",\ q}} \lambda_q \leq \delta_b \ \forall\ b \in \mathscr{B} \tag{33}$$

$$\text{eqLink1} \sum_{q \mid \mathit{not}\mathscr{I}_{b,\ "1",\ q}} \lambda_q \leq 1 - \delta_b \ \forall\ b \in \mathscr{B} \tag{34}$$

Finally, an additional constraint (35) is necessary to ensure that the interpolation factor between two segments always sums up to one. Set PWL_q keeps track of the amount of segments a cost function has and allows to deal with a varying segment count in the same formulation.

$$\text{eqSumLambda} \sum_q \lambda_q \cdot \mathscr{L}_q = 1 \tag{35}$$

Piecewise capture interpolation

$$eqCC^{link0}_{tc,c,b} \sum_{q \mid not\mathscr{T}^{CC}_{c,\,b,\,"0",\,q}} \lambda^{Cc}_{tc,c,q} \le \delta^{Cc}_{tc,c,b} \;\forall (tc,c,b) \in (\mathscr{T}c,\,\mathscr{C},\mathscr{B}) \tag{36}$$

$$eqCC^{link1}_{tc,c,b} \sum_{q \mid not\mathscr{T}^{CC}_{c,\,b,\,"1",\,q}} \lambda^{Cc}_{tc,c,q} \le 1 - \delta^{Cc}_{tc,c,b} \;\forall\; (tc,c,b) \in (\mathscr{T}c,\,\mathscr{C},\mathscr{B}) \tag{37}$$

$$\text{eqSumLambda}^{CC}_{tc,c} \sum_{q} \lambda^{CC}_{tc,c,q} \cdot \mathscr{L}^{Cc}_{tc,q} = 1 \;\forall\; (tc,c) \in (\mathscr{T}c,\,\mathscr{C}) \tag{38}$$

Piecewise transport interpolation

$$\text{eqT}^{link0}_{t^*,t^*,b} \sum_{q \mid not\mathscr{T}^{T}_{t^*,t^*,\,b,\,"0",\,q}} \lambda^{T}_{t^*,t^*,q} \le \delta^{T}_{t^*,t^*,b} \;\forall\; (t^*,\;t^*,b) \in\; (t^*,\;t^*,\;\mathscr{B}) \tag{39}$$

$$\text{eqT}^{link1}_{t^*,t^*,b} \sum_{q \mid not\mathscr{T}^{T}_{t^*,t^*,\,b,\,"1",\,q}} \lambda^{T}_{t^*,t^*,q} \le 1 - \delta^{T}_{t^*,t^*,b} \;\forall\; (t^*,t^*,\;b) \in\; (\;t^*,\;t^*,\mathscr{B}) \tag{40}$$

$$\text{eqSumLambda}^{T}_{t^*,t^*} \sum_{q} \lambda^{T}_{t^*,t^*,q} \cdot \mathscr{L}^{Bp}_{t^*,t^*,q} = 1 \;\forall (t^*,t^*) \Big|\; \mathscr{L}^{Flow}_{t^*,t^*} \tag{41}$$

Piecewise electrolyzer interpolation

$$\text{eqEle}^{link0}_{e,b} \sum_{q \mid not\mathscr{T}^{Ele}_{e,\,b,\,"0",\,q}} \lambda^{Ele}_{e,q} \le \delta^{Ele}_{e,b} \;\forall\; (e,b) \;\in\; (\mathscr{E},\mathscr{B}) \tag{42}$$

$$\text{eqEle}^{link1}_{e,b} \sum_{q \mid not\mathscr{T}^{Ele}_{e,\,b,\,"1",\,q}} \lambda^{Ele}_{e,q} \le 1 - \delta^{Ele}_{e,b} \;\forall (e,b) \in (\mathscr{E},\mathscr{B}) \tag{43}$$

$$\text{eqSumLambda}^{Ele}_{e} \sum_{q} \lambda^{Ele}_{e,q} = 1 \;\forall\; (e) \;\in (\mathscr{E}) \tag{44}$$

Appendix III – Optimality gap

The remaining optimality gap for the market fulfillment from 50 % onwards is presented in Fig. 19. This range up to and including 65 % market fulfillment was always solved until the optimality tolerance within the six-hour window for all scenarios. Between 70 % and 95 % syngas market fulfillment, the model was solved below a 0.25 % optimality gap for all scenarios.

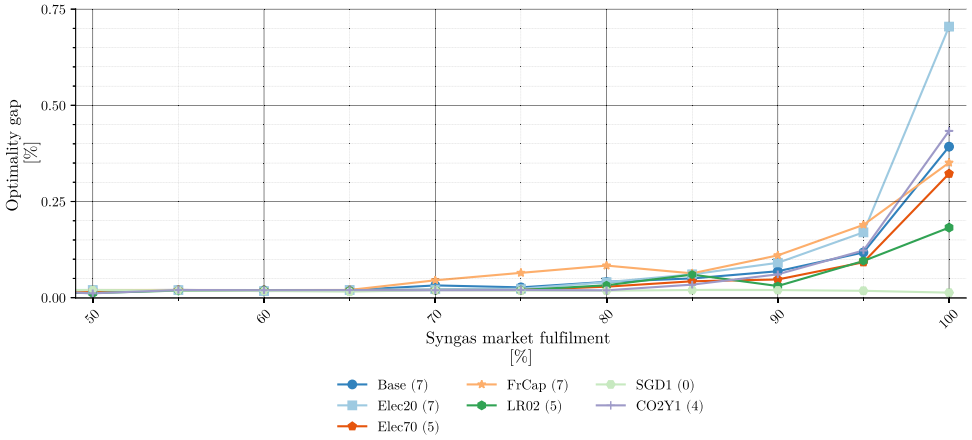

Fig. 19. The optimality gap across the different parameter explorations, the number in between brackets indicates the number of optimizations that did not reach the optimality tolerance of 0.02 %.

The optimality gap was the highest at 100 % market fulfillment, below 0.75 % for all runs. Proving optimality was the most challenging at this market fulfilment percentage. At 100 %, the highest number of feasible SC configurations are possible. Furthermore, there was a wide range in the size of syngas demands that the model needed to fulfill. Also at smaller flows, where the electrolyzer scaled in the non-linear regime via the piecewise linear approximation. In this case, many branches must be explored to solve the electrolyzer scaling, contributing to a larger optimality gap within the allotted solving time.

Typically, between 4 and 7 market fulfilments were not solved to the optimality tolerance within the chosen time window. Relaxing the syngas demand constraint in the scenario SGD1 eased the optimization since all the market fulfilments were solved until the optimality tolerance.

Data availability

GIS-based data, input CO_2 sources, output syngas demands, European-wide terrain rasters, and runnable GAMS models with input files are available at: doi.org/10.5281/zenodo.15178217

References

Abdelshafy, A., Walther, G., 2022. Coupling carbon capture and utilization with the construction industry: opportunities in Western Germany. J. CO2 Util. 57. https://doi.org/10.1016/j.jcou.2021.101866.

Al Ghafri, S.Z., Munro, S., Cardella, U., Funke, T., Notardonato, W., Trusler, J.P.M., Leachman, J., Span, R., Kamiya, S., Pearce, G., Swanger, A., Rodriguez, E.D., Bajada, P., Jiao, F., Peng, K., Siahvashi, A., Johns, M.L., May, E.F., 2022. Hydrogen liquefaction: a review of the fundamental physics, engineering practice and future opportunities. Energy Environ. Sci. 15, 2690–2731. https://doi.org/10.1039/d2ee00099g.

Almena, A., Fryer, P.J., Bakalis, S., Lopez-Quiroga, E., 2019. Centralized and distributed food manufacture: a modeling platform for technological, environmental and economic assessment at different production scales. Sustain. Prod. Consum. 19, 181–193. https://doi.org/10.1016/j.spc.2019.03.001.

Andersen, D.N., Slothuus, T., Larsen, P.B., 2014. Survey of Formaldehyde.

Bello, S., Galán-Martín, Á., Feijoo, G., Moreira, M.T., Guillén-Gosálbez, G., 2020. BECCS based on bioethanol from wood residues: potential towards a carbon-negative transport and side-effects. Appl. Energy 279, 115884. https://doi.org/10.1016/j.apenergy.2020.115884.

Bennæs, A., Skogset, M., Svorkdal, T., Fagerholt, K., Herlicka, L., Meisel, F., Rickels, W., 2024. Modeling a supply chain for carbon capture and offshore storage—a German–Norwegian case study. Int. J. Greenh. Gas Control 132, 104028. https://doi.org/10.1016/j.ijggc.2023.104028.

Bisinella, V., Hulgaard, T., Riber, C., Damgaard, A., Christensen, T.H., 2021. Environmental assessment of carbon capture and storage (CCS) as a post-treatment technology in waste incineration. Waste Manag. 128, 99–113. https://doi.org/10.1016/j.wasman.2021.04.046.

Bjerketvedt, V.S., Tomasgard, A., Roussanaly, S., 2022. Deploying a shipping infrastructure to enable carbon capture and storage from Norwegian industries. J. Clean. Prod. 333, 129586. https://doi.org/10.1016/j.jclepro.2021.129586.

Bui, M., Zhang, D., Fajardy, M., Mac Dowell, N., 2021. Delivering carbon negative electricity, heat and hydrogen with BECCS – comparing the options. Int. J. Hydrogen Energy 46, 15298–15321. https://doi.org/10.1016/j.ijhydene.2021.02.042.

Bushuyev, O.S., De Luna, P., Dinh, C.T., Tao, L., Saur, G., van de Lagemaat, J., Kelley, S.O., Sargent, E.H., 2018. What should we make with CO2 and how can we make it? Joule 2, 825–832. https://doi.org/10.1016/j.joule.2017.09.003.

Chandra, C., Grabis, J., 2016. Supply chain configuration: Concepts, solutions, and applications, Supply Chain Configuration: Concepts, Solutions, and Applications, Second Edition. https://doi.org/10.1007/978-1-4939-3557-4.

Choe, C., Cheon, S., Gu, J., Lim, H., 2022. Critical aspect of renewable syngas production for power-to-fuel via solid oxide electrolysis: Integrative assessment for potential renewable energy source. Renew. Sustain. Energy Rev. 161, 112398. https://doi.org/10.1016/j.rser.2022.112398.

Cormos, C.C., 2014. Renewable hydrogen production concepts from bioethanol reforming with carbon capture. Int. J. Hydrogen Energy 39, 5597–5606. https://doi.org/10.1016/j.ijhydene.2014.01.114.

Cui, S., Yu, C., Tan, X., Huang, H., Yao, X., Qiu, J., 2020. Achieving multiple and tunable ratios of syngas to meet various downstream industrial processes. ACS Sustain. Chem. Eng. 8, 3328–3335. https://doi.org/10.1021/acssuschemeng.9b07255.

d'Amore, F., Romano, M.C., Bezzo, F., 2021. Optimal design of European supply chains for carbon capture and storage from industrial emission sources including pipe and ship transport. Int. J. Greenh. Gas Control 109. https://doi.org/10.1016/j.ijggc.2021.103372.

de Kleijne, K., Hanssen, S.V., van Dinteren, L., Huijbregts, M.A.J., van Zelm, R., de Coninck, H., 2022. Limits to Paris compatibility of CO2 capture and utilization. One Earth 5, 168–185. https://doi.org/10.1016/j.oneear.2022.01.006.

Deka, D.J., Kim, J., Gunduz, S., Ferree, M., Co, A.C., Ozkan, U.S., 2020. Temperature-induced changes in the synthesis gas composition in a high-temperature H2O and CO2 co-electrolysis system. Appl. Catal. A Gen. 602, 117697. https://doi.org/10.1016/j.apcata.2020.117697.

Delft High Performance Computing Centre (DHPC), 2022. Delft Blue Supercomputer (Phase 1).

Detz, R.J., Ferchaud, C.J., Kalkman, A.J., Kemper, J., Sánchez-Martínez, C., Saric, M., Shinde, M.V., 2023. Electrochemical CO2 conversion technologies: state-of-the-art and future perspectives. Sustain. Energy Fuels 7, 5445–5472. https://doi.org/10.1039/d3se00775h.

Diettrich, J., Pluta, A., Medjroubi, W., 2021. SciGRID_gas IGGIELGN (1.1.2) [Data set]. https://doi.org/10.5281/zenodo.4767098.

Ester, M., Kriegel, H.P., Sander, J., Xu, X., 1996. A density-based algorithm for discovering clusters a density-based algorithm for discovering clusters in large spatial databases with noise. In: Proceedings - 2nd International Conference on Knowledge Discovery and Data Mining, KDD 1996, pp. 226–231.

European Biogas Association, 2023. Statistical Report 2023, Definitions.

European Biogas Association, Gas Infrastructure Europe, 2021. Biomethane Map 2021.

European Commission, 2019. The European green deal. Eur. Comm. 53, 24. https://doi.org/10.1017/CBO9781107415324.004.

European Environment Agency, 2024. EEA greenhouse gases - Data viewer [WWW Document]. URL https://www.eea.europa.eu/data-and-maps/data/data-viewers/greenhouse-gases-viewer (accessed 9.18.24).

European Environment Agency, 2023. The European Pollutant Release and Transfer Register (E-PRTR).

European Environment Agency, 2021a. Natura 2000 data - the European network of protected sites.

European Environment Agency, 2021b. Nationally designated areas.

European Environment Agency, 2019a. CORINE Land Cover 2018.

European Environment Agency, 2019b. Natura 2000 data - the European network of protected sites.

European Environment Agency, 2012. Preliminary version of a DEM over Europe from the GSGRDA project (EU-DEM-PRE, resolution 25 m).

European Industrial Gases Association AISBL, 2014. Carbon monoxide and syngas pipeline system.

Eurostat, 2024a. Electricity prices for household consumers - bi-annual data (from 2007 onwards). Data Brows.

Eurostat, 2024b. Exchange rates and interest rates.

Haaf, M., Anantharaman, R., Roussanaly, S., Ströhle, J., Epple, B., 2020. CO2 capture from waste-to-energy plants: Techno-economic assessment of novel integration concepts of calcium looping technology. Resour. Conserv. Recycl. 162, 104973. https://doi.org/10.1016/j.resconrec.2020.104973.

Hasan, M.M.F., Baliban, R.C., Elia, J.A., Floudas, C.A., 2012. Modeling, simulation, and optimization of postcombustion CO2 capture for variable feed concentration and flow rate. 1. Chemical absorption and membrane processes. Ind. Eng. Chem. Res. 51, 15642–15664. https://doi.org/10.1021/ie301571d.

Hasan, M.M.F., Boukouvala, F., First, E.L., Floudas, C.A., 2014. Nationwide, regional, and statewide CO2 capture, utilization, and sequestration supply chain network optimization. Ind. Eng. Chem. Res. 53, 7489–7506. https://doi.org/10.1021/ie402931c.

Hughes, S., Zoelle, A., Woods, M., Henry, S., Homsy, S., Pidaparti, S., Kuehn, N., Hoffman, H., Forrest, K., Sheriff, A., Fout, T., Summers, W., Herron, S., 2022. Cost of Capturing CO2 from Industrial Sources. United States.

ICIS, 2023a. Chemical Profile: Europe methanol. ICIS Chemical Business.

ICIS, 2023b. Chemical profile : Europe ethanol. ICIS Chemical Business Chemical.

ICIS, 2023c. Chemical profile: Europe acetic acid. ICIS Chemical Business.

ICIS, 2023d. Chemical Profile: Europe MDI. ICIS Chemical Business.

ICIS, 2022. Chemical profile : Europe oxo-alcohols. ICIS Chemical Business Chemical.

ICIS, 2020. Chemical profile : Europe ethanol.

ICIS, 2018. Chemical Profile: Europe MTBE. ICIS Chemical Business.

ICIS, 2017. Chemical Profile: Europe Butanediol. ICIS Chemical Business Chemical.

IEA Bioenergy Task 37, 2020. Biogas upgrading plants.

IEA Bioenergy Task 39, 2023. Database on facilities for the production of advanced liquid and gaseous biofuels for transport [WWW Document].

IEAGHG, 2018. Effects of plant location on cost of CO2 capture. https://doi.org/10.2139/ssrn.3365621.

Jarvis, S.M., Samsatli, S., 2018. Technologies and infrastructures underpinning future CO2 value chains: a comprehensive review and comparative analysis. Renew. Sustain. Energy Rev. 85, 46–68. https://doi.org/10.1016/j.rser.2018.01.007.

Kalvelagen, E., 2019. Piecewise linear functions and formulations for interpolation (part 3) [WWW Document]. Yet another math Program. Consult. URL https://yetanothermathprogrammingconsultant.blogspot.com/2019/03/piecewise-linear-functions-and.html.

Kearns, D.T., 2019. Waste-to-Energy with CCS: a Pathway to Carbon-Negative Power Generation. Global CCS Institute.

Knauff, H.W., 1973. Location, size, and interaction of chemical plants. Environmental Engineering. Springer Netherlands, Dordrecht, pp. 43–52. https://doi.org/10.1007/978-94-010-2608-6_5.

Knoope, M., Guijt, W., Ramírez, A., Faaij, A., 2014a. Improved cost models for optimizing CO2 pipeline configuration for point-to-point pipelines and simple networks. Int. J. Greenh. Gas Control 22, 25–46. https://doi.org/10.1016/j.ijggc.2013.12.016.

Knoope, M., Raben, I., Ramírez, A., Spruijt, M., Faaij, A., 2014b. The influence of risk mitigation measures on the risks, costs and routing of CO2 pipelines. Int. J. Greenh. Gas Control 29, 104–124. https://doi.org/10.1016/j.ijggc.2014.08.001.

Laporte, G., Nickel, S., 2015. Location Science, Location Science. https://doi.org/10.1007/978-3-319-13111-5.

Laude, A., Ricci, O., Bureau, G., Royer-Adnot, J., Fabbri, A., 2011. CO2 capture and storage from a bioethanol plant: carbon and energy footprint and economic assessment. Int. J. Greenh. Gas Control 5, 1220–1231. https://doi.org/10.1016/j.ijggc.2011.06.004.

Lorenzo, M., Díaz, M., 2022. Preliminary EU CO2 Sources.

McCollum, D.L., Ogden, J.M., 2006. Techno economic model for carbon dioxide compression, transport and storage and correlations for estimating carbon dioxide density and viscosity.

McCoy, S.T., Rubin, E.S., 2008. An engineering-economic model of pipeline transport of CO2 with application to carbon capture and storage. Int. J. Greenh. Gas Control 2, 219–229. https://doi.org/10.1016/S1750-5836(07)00119-3.

Morgan, D., Guinan, A., Sheriff, A., 2023. FECM/NETL CO2 Transport Cost Model (2023): Description and User's Manual. United States.

Morgenthaler, S., Kuckshinrichs, W., Witthaut, D., 2020. Optimal system layout and locations for fully renewable high temperature co-electrolysis. Appl. Energy 260, 114218. https://doi.org/10.1016/j.apenergy.2019.114218.

Muggeo, V.M.R., 2003. Estimating regression models with unknown break-points. Stat. Med. 22, 3055–3071. https://doi.org/10.1002/sim.1545.
Noordende, H.V., Berkel, F.V., Stodolny, M., 2023. Next level solid oxide electrolysis. Inst. Sustain. Process Technol.
Onarheim, K., Kangas, P., Kaijaluoto, S., Hankalin, V., Santos, S., 2016. Evaluation of retrofitting CCS in a market pulp and integrated pulp, IEAGHG.
Onarheim, K., Santos, S., Kangas, P., Hankalin, V., 2017. Performance and costs of CCS in the pulp and paper industry part 1: performance of amine-based post-combustion CO2 capture. Int. J. Greenh. Gas Control 59, 58–73. https://doi.org/10.1016/j.ijggc.2017.02.008.
Ostovari, H., Kuhrmann, L., Mayer, F., Minten, H., Bardow, A., 2023. Towards a European supply chain for CO2 capture, utilization, and storage by mineralization: Insights from cost-optimal design. J. CO2 Util. 72. https://doi.org/10.1016/j.jcou.2023.102496.
Pilgrim, C., 2021. piecewise-regression (aka segmented regression) in Python. J. Open Source Softw. 6, 3859. https://doi.org/10.21105/joss.03859.
Prosser, J.H., James, B.D., Murphy, B.M., Wendt, D.S., Casteel, M.J., Westover, T.L., Knighton, L.T., 2024. Cost analysis of hydrogen production by high-temperature solid oxide electrolysis. Int. J. Hydrogen Energy 49, 207–227. https://doi.org/10.1016/j.ijhydene.2023.07.084.
Raya-Imbernón, A., Samu, A.A., Barwe, S., Cusati, G., Fődi, T., Hepp, B.M., Janáky, C., 2024. Renewable syngas generation via low-temperature electrolysis: opportunities and challenges. ACS Energy Lett. 9, 288–297. https://doi.org/10.1021/acsenergylett.3c02446.
Ridjan, I., 2015. Integrated electrofuel and renewable energy systems.
Rodin, V., Lindorfer, J., Böhm, H., Vieira, L., 2020. Assessing the potential of carbon dioxide valorisation in Europe with focus on biogenic CO2. J. CO2 Util. 41, 101219. https://doi.org/10.1016/j.jcou.2020.101219.
Sagues, W.J., Jameel, H., Sanchez, D.L., Park, S., 2020. Prospects for bioenergy with carbon capture & storage (BECCS) in the United States pulp and paper industry. Energy Environ. Sci. 13, 2243–2261. https://doi.org/10.1039/d0ee01107j.
Schiffer, Z.J., Manthiram, K., 2017. Electrification and decarbonization of the chemical industry. Joule 1, 10–14. https://doi.org/10.1016/j.joule.2017.07.008.
Schreiber, A., Peschel, A., Hentschel, B., Zapp, P., 2020. Life cycle assessment of power-to-syngas: comparing high temperature co-electrolysis and steam methane reforming. Front. Energy Res. 8, 533850. https://doi.org/10.3389/fenrg.2020.533850.
Serpa, J., Morbee, J., Tzimas, E., 2011. Technical and economic characteristics of a CO2 transmission pipeline infrastructure. https://doi.org/10.2790/30861.
Smith, E., Morris, J., Kheshgi, H., Teletzke, G., Herzog, H., Paltsev, S., 2021. The cost of CO2 transport and storage in global integrated assessment modeling. Int. J. Greenh. Gas Control 109, 103367. https://doi.org/10.1016/j.ijggc.2021.103367.
Smith, W.A., Burdyny, T., Vermaas, D.A., Geerlings, H., 2019. Pathways to industrial-scale fuel out of thin air from CO2 electrolysis. Joule 3, 1822–1834. https://doi.org/10.1016/j.joule.2019.07.009.
Sorknæs, P., Johannsen, R.M., Korberg, A.D., Nielsen, T.B., Petersen, U.R., Mathiesen, B. V., 2022. Electrification of the industrial sector in 100 % renewable energy scenarios. Energy 254, 124339. https://doi.org/10.1016/j.energy.2022.124339.
Stolecka, K., Rusin, A., 2020. Analysis of hazards related to syngas production and transport. Renew. Energy 146, 2535–2555. https://doi.org/10.1016/j.renene.2019.08.102.
van den Broek, M., Mesquita, P., Carneiro, J., Silva, J.R., Berghout, N., Ramírez, A., Gouveia, J.P., Seixas, J., Cabal, H., Martinez, R., Rimi, A., Zarhloule, Y., Sardinha, M., Boavida, D., Tosato, G.C., 2013. Region specific challenges of a CO2 pipeline infrastructure in the west Mediterranean area model results versus stakeholder views. Energy Proc. 37, 3137–3146. https://doi.org/10.1016/j.egypro.2013.06.200.
van der Spek, M., Roussanaly, S., Rubin, E.S., 2019. Best practices and recent advances in CCS cost engineering and economic analysis. Int. J. Greenh. Gas Control 83, 91–104. https://doi.org/10.1016/j.ijggc.2019.02.006.
Vieira, L., 2018. CO2EXIDE - CO2-based Electrosynthesis of ethylene oXIDE.
Wang, N., Wang, D., Krook-Riekkola, A., Ji, X., 2023. MEA-based CO2 capture: a study focuses on MEA concentrations and process parameters. Front. Energy Res. 11, 1–15. https://doi.org/10.3389/fenrg.2023.1230743.
Weber, M., Perrin, J., 2008. Hydrogen Transport and Distribution. Hydrogen Technol. 129–149. https://doi.org/10.1007/978-3-540-69925-5_4.
Wilkes, M.D., Ejeh, J., Roberts, D., Brown, S., 2023. Cost of small-scale dispatchable CO2 capture: techno-economic comparison and case study evaluation. Int. J. Greenh. Gas Control 127, 103931. https://doi.org/10.1016/j.ijggc.2023.103931.